Variations in O_3, CO, and CH_4 over the Bay of Bengal during the summer monsoon season: Ship-borne measurements and model simulations

Imran A. Girach[1,2], Narendra Ojha[2], Prabha R. Nair[1], Andrea Pozzer[2], Yogesh K. Tiwari[3], K. Ravi Kumar[4,5], and Jos Lelieveld[2]

[1]Space Physics Laboratory, Vikram Sarabhai Space Centre, Thiruvananthapuram 695022, India

[2]Department of Atmospheric Chemistry, Max Planck Institute for Chemistry, Mainz 55128, Germany

[3]Indian Institute of Tropical Meteorology, Pune 411 008, India

[4]National Institute of Polar Research, Tachikawa, Japan

[5]Department of Environmental Geochemical Cycle Research, JAMSTEC, Yokohama, Japan

Correspondence to: Imran A. Girach (imran.girach@gmail.com) and Narendra Ojha (narendra.ojha@mpic.de)

Abstract

We present ship-borne measurements of surface ozone (O_3), carbon monoxide (CO) and methane (CH_4) over the Bay of Bengal (BoB), the first time such measurements have been performed during the summer monsoon season, as a part of the Continental Tropical Convergence Zone (CTCZ) experiment during 2009. O_3, CO, and CH_4 mixing ratios exhibited significant spatial and temporal variability in the ranges of 8–54 nmol mol^{-1}, 50–200 nmol mol^{-1}, and 1.57–2.15 µmol mol^{-1}, with means of 29.7±6.8 nmol mol^{-1}, 96±25 nmol mol^{-1}, and 1.83±0.14 µmol mol^{-1}, respectively. The average mixing ratios of trace gases over BoB in airmasses from central/northern India (O_3: 30±7 nmol mol^{-1}, CO: 95±25 nmol mol^{-1}, CH_4: 1.86±0.12 µmol mol^{-1}), were not statistically different from those in airmasses from southern India (O_3: 27±5 nmol mol^{-1}, CO: 101±27 nmol mol^{-1}, CH_4: 1.72±0.14 µmol mol^{-1}). Spatial variability is observed to be most significant for CH_4 with higher mixing ratios in the airmasses from central/northern India, where higher CH_4 levels are seen in the SCIAMACHY (SCanning Imaging Absorption spectroMeter for Atmospheric CartograpHY) data. O_3 mixing ratios over the BoB showed large reductions (by ~20 nmol mol^{-1}) during four rainfall events. Temporal changes in the meteorological parameters, in conjunction with O_3 vertical profile, indicate that these low O_3 events are associated with downdrafts of free-tropospheric O_3-poor airmasses. While the observed variations of O_3 and CO are successfully reproduced using the Weather Research and Forecasting model with Chemistry (WRF-Chem), this model overestimates mean concentrations by about 6 and 16% for O_3 and CO respectively, generally overestimating O_3 mixing ratios during the rainfall events. An analysis of modeled O_3 along airmass trajectories show mean en route O_3 production rate of about 4.6 nmol mol^{-1} day^{-1} in the outflow towards the BoB. Analysis of the various tendencies from model simulations during an event on August 10,

2009, reproduced by the model, shows horizontal advection rapidly transporting O_3-rich airmasses from near the coast across the BoB. This study fills a gap in the availability of trace gas measurements over the BoB, and when combined with data from previous campaigns, reveals large seasonal amplitude (~39 and ~207 nmol mol^{-1} for O_3 and CO, respectively) over the northern BoB.

1. Introduction

Tropospheric ozone (O_3) is the third most important greenhouse gas, contributing to global warming and climate change with a radiative forcing of 0.40±0.20 Wm^{-2} (IPCC 2013). O_3 is also a pivotal trace gas in tropospheric chemistry, as it is a major source of hydroxyl radical (OH), which removes most of the organic compounds and pollutants from the atmosphere and controls the oxidation capacity of the troposphere (e.g. Brasseur et al., 1999; Finlayson-Pitts and Pitts, 2003; Seinfeld and Pandis, 2006). Further, enhanced concentrations of surface O_3 have detrimental effects on human health and vegetation (Heagle, 1989; Seinfeld and Pandis, 2006). Approximately 80% of tropospheric O_3 is produced by in situ photochemical reactions in the presence of nitrogen oxides (NO_x = NO + NO_2) involving the precursor gases of methane, non-methane hydrocarbons (NMHCs), and CO (Fishman et al., 1979; Crutzen et al., 1999; Seinfeld and Pandis, 2006). The remaining 20% of tropospheric O_3 is attributed to intrusions of stratospheric air during frontal activities or to tropopause folding events (Lelieveld and Dentener, 2000; Sprenger et al., 2007). Depending upon meteorological conditions and the availability of the aforementioned precursors, a net production or destruction of O_3 prevails. The average lifetime of O_3 is about one week in the lower troposphere, which leads to large variability in its spatial and temporal distributions, as compared to the long-lived greenhouse gases. The budget of tropospheric O_3 and its implications for human health, crop yields, and climate are, however, not yet well quantified, especially over regions in Asia. This is mainly due to a lack of in situ measurements (e.g. Cooper et al., 2014; Monks et al., 2015).

Carbon monoxide (CO) is an indirect greenhouse gas which also has adverse effects on the health of humans and animals (WHO 1999). Although it does not have a direct greenhouse effect like methane and carbon dioxide, its role in atmospheric chemistry is estimated to cause an indirect radiative forcing of 0.23 (0.18–0.29) Wm^{-2} (IPCC 2013). The major sources of CO are fossil fuel combustion, biomass burning, and oxidation of hydrocarbons such as CH_4 and isoprene (e.g. Jacob, 1999; Bergamaschi et al., 2000; Seinfeld and Pandis, 2006).

Methane (CH_4) is one of the major greenhouse gases, with a direct radiative forcing of 0.48±0.05 Wm^{-2} (IPCC 2013). This gas plays a major role in the climate and in atmospheric chemistry. CH_4 is emitted from variety of natural and anthropogenic sources (Jacob, 1999) and is removed primarily through its reaction with OH radicals (Fung et al., 1991, Seinfeld and Pandis, 2006).

The marine regions adjoining South Asia have been observed to have elevated levels of surface O_3 due to the outflow of continental pollution (Lawrence and Lelieveld, 2010) and minimal chemical loss by titration (e.g. Lal and Lawrence, 2001; Ojha et al., 2012). Suggested sources for this elevated O_3 and other trace gases observed over the marine regions surrounding India are anthropogenic, biomass burning, and biogenic emissions over continental India

(Naja et al., 2004; Lawrence and Lelieveld, 2010; Nair et al., 2011; David et al., 2011). The airmasses influenced by continental emissions undergo chemical transformation, including O_3 production, during their transport to the cleaner marine regions. In situ measurements over the marine regions are required to understand the effects of direct outflow, en route chemical transformation, and the chemistry in the transported airmasses. (Lawrence and Lelieveld, 2010, and references therein).

The experiments that have been conducted to date over the marine environment adjacent to the Indian region have revealed considerable spatial heterogeneity in the distribution of trace gases and aerosols, influences from source regions such as the Indo-Gangetic Plains (IGP), and radiative impacts (Nair et al., 2011; David et al., 2011; Mallik et al., 2013; Moorthy et al., 2009; Nair et al., 2010). Observations made during the Indian Ocean Experiment (INDOEX; Lal and Lawrence, 2001) and model simulations (Ojha et al., 2012) both found the O_3 mixing ratios over these remote marine regions to be even higher than those over the upwind continental regions, due to complex O_3 chemistry. Lawrence and Lelieveld (2010) provided a detailed review of the outflow of trace gases and aerosols from South Asia to the surrounding marine regions. Transport of airmasses between the Indian subcontinent and the adjacent marine regions has strong seasonal dependence associated with the monsoonal circulation (e.g. Kumar et al., 2015).

The marine environment of the Bay of Bengal (BoB), the largest bay in the world, is surrounded by landmasses on three sides, making it highly suitable to observe enhanced concentrations of trace species. Further, seasonal changes in synoptic winds make this a unique region to study variations in trace species due to transport and en route photochemistry. Considering the aforementioned special characterisitics of the BoB, as well as the considerable heterogeneity of trace gas and aerosol distribution, in situ measurements covering large areas are essential for investigating the distribution of pollutants and the controlling processes. Extensive in situ measurements of various trace gases over the BoB have been conducted in the following field campaigns: INDOEX during the winter months of 1998 and 1999 (Lelieveld et al., 2001; Muhle et al., 2002); the Integrated Campaign for Aerosols, gases, and Radiation Budget (ICARB) during the March–May (pre-monsoon season) of 2006 (Nair et al., 2011; Srivastava et al., 2011; Srivastava et al., 2012); the winter-ICARB (W-ICARB) during December–January 2009 (Girach and Nair, 2010; 2014; David et al., 2011); the Bay of Bengal Experiment (BOBEX)-I during February–March 2001 (Lal et al., 2006); the Bay of Bengal Process Studies (BOBPS) during September–October 2002 (Sahu et al., 2006); BOBEX–II during February 2003 (Lal et al., 2007); and the other campaign conducted during October–November 2010 (Mallik et al., 2013).

Although earlier studies have covered the spatio-temporal distribution of trace gases during most seasons over the BoB, there is still a lack of observations over the BoB during the summer monsoon season (June–August). The Asian summer monsoon circulation provides a pathway for pollution transport into the stratosphere (Randel et al., 2010), and observations taken during monsoon season capture a time of high water-vapour loading over the BoB. Deep convection during the summer monsoon can uplift boundary layer pollution to higher altitudes, which is then distributed over a larger region, thereby influencing air quality and climate over much larger regions (Lawrence and Lelieveld, 2010), extending as far as, for example, over the Mediterranean (e.g. Lelieveld et al., 2002; Scheeren et al., 2003). Such in situ measurements are also essential given the fact that satellite remote sensing of boundary layer

O_3 has relatively higher uncertainty. The uncertainties in satellite retrievals of trace species are particularly high during the summer monsoon season, as the view of satellite instruments is frequently obscured by thick clouds.

In the present paper, the ship-based measurements of surface O_3, CO, and CH_4 over the BoB are presented for the summer monsoon season of 2009. These observations were carried out as a part of the Continental Tropical Convergence Zone (CTCZ) experiment (http://odis.incois.gov.in/index.php/project-datasets/ctcz-programme) under the Indian Climate Research Programme (ICRP) of the Government of India. In this study, the spatial and temporal variations of O_3 over the BoB and the effects of transport are analysed. These observations are compared with simulations from a regional model, Weather Research and Forecasting coupled with Chemistry (WRF-Chem). The sharp reductions observed in O_3 during rainfall events are investigated in greater detail.

2. The cruise track and background conditions

Figure 1 shows the cruise track of the Oceanic Research Vessel (ORV) *Sagar Kanya* during the CTCZ campaign (cruise number SK 261). The arrows marked on the track show the direction of the ship, which sailed from Chennai (80.3° E, 13.1° N, marked by a circle) on July 16, 2009. The cruise offered greater coverage in the northern BoB than the southern or central BoB areas. To take time series measurements, the ship was kept stationary for fifteen days (July 22 to August 06, 2009) at 89° E, 19° N as marked by a triangle in the figure. After several tracks, covering latitude sector 11.0 to 21.1° N and longitude sector 80.3 to 90.1° E, the cruise ended on August 17, 2009 at Chennai, for a total of 32 days of voyage. The average wind pattern at 925 hPa (NCEP/NCAR reanalysis; http://www.esrl.noaa.gov/psd) during the cruise period is shown in Figure 1. The prevailing westerly and southwesterly winds transport O_3 and its precursors from the Indian landmass to the BoB during study period. The spatial distribution of emissions of NO_x, an O_3 precursor gas, is also shown as colour map in Fig. 1. NO_x emissions are obtained from the Intercontinental Chemical Transport Experiment – Phase B (INTEX-B) inventory (Zhang et al., 2009), which is representative of the year 2006. NO_x emissions are relatively higher over parts of eastern and southern India as compared to central India. The square tagged with Thiruvananthapuram shows the location corresponding to the measurements shown in Fig. 9.

3. Experimental details and data

Surface O_3 measurements were carried out using an online ultraviolet (UV) photometric ozone analyzer (Model O3 42), manufactured by Environnement S.A, France. The analyser utilises the absorption of UV radiation by O_3 molecules at 253.7 nm and derives O_3 mixing ratios using the Beer–Lambert law. This UV absorption-based analyser has an uncertainty of about 5% (Tanimoto, 2007), corresponding to ~1.5 nmol mol^{-1} for the observed range of O_3. Zero noise of the instrument is 0.5 nmol mol^{-1}. The instrument has a lower detection limit of 1 nmol mol^{-1} and a linearity of ±1%. An individual measurement is performed at a minimum response time of 10 seconds. The analyzer was operated on auto-response mode, whereby responses could be 10–90 seconds depending upon changes in O_3 mixing ratios. However, data were recorded continuously at 5-minute intervals.

CO measurements were made using an online CO analyzer (Model CO12 Module) manufactured by Environnement S.A, France. This instrument works on the principle of Non-Dispersive Infrared (NDIR) absorption by CO molecules at the wavelength of 4.67 µm. The instrument has a lower detection limit of 50 nmol mol^{-1}, a linearity of 1%, and a response time of 40 seconds. The overall uncertainty in hourly CO measurements is estimated to be ~ 10% at a CO value of 150 nmol mol^{-1} (Sawa et al., 2007; Tanimoto et al., 2007).

Air was drawn from a height of approximately 15 meter above the sea surface through a Teflon tube. Before and after the cruise, both analyzers were calibrated, with calibration factors not found to be significantly changed. The calibrations of both analysers were carried out using appropriate calibration standards traceable to NIST and a multi-channel calibrator, following the procedure mentioned in the manuals of analysers. While O_3 analyser was calibrated for mixing ratios of 30 nmol mol^{-1}, the CO analyser was calibrated for mixing ratios of 1.1 µmol mol^{-1}. Meteorological parameters such as pressure, temperature, and relative humidity were measured continuously onboard the ship. Trace gas measurements affected by the ship exhaust were identified and discarded using onboard wind direction and NO_x measurements.

In addition, a total of 29 air samples were collected in 1-liter glass flasks during the cruise and were analyzed for CH_4 using a Gas Chromatograph (GC) coupled with a Flame Ionization Detector (FID), as described in Tiwari and Ravi Kumar (2011). These CH_4 measurements are traceable to the WMO standard scale. CH_4 standards were obtained from the WMO Central Calibration Laboratory (CCL) at the National Oceanic and Atmospheric Administration (NOAA)/Earth System Research Laboratory (ESRL)/Global Monitoring Division (GMD), located in Boulder, Colorado, USA. The precision for CH_4 measurements was approximately ±0.1 µmol mol^{-1}. A detailed description of the analytical procedure for CH_4 measurement and calibration of GC is given in Ravikumar et al. (2014).

To further study the observed low-O_3 events over BoB, measurements made at Thumba, Thiruvananthapuram are used as a case study. Using the same O_3 analyzer as the one used for surface O_3 measurements over BoB, continuous measurements of surface O_3 were taken at Thumba, Thiruvananthapuram (David and Nair, 2011; Girach et al., 2012) in July 2011. Along with various meteorological parameters, rainfall measurements were also taken at Thumba at 5-minute of integration time using an automatic weather station manufactured by Dynalab Weathertech Pvt. Ltd, India. The site, Thumba, is situated just ~500 m away from the west coast, with sandy terrain, and is a less populated area in the city of Thiruvananthapuram (8.5° N, 76.9° E) at southern tip of India. For more details about the Thumba site and measurements please see, for example, Nair et al. (2002) and David and Nair (2011).

A vertical profile of O_3 was measured on July 28, 2011 at Thumba using an electrochemical concentration cell ozonesonde (EN-SCI 2ZV7 ECC; Komhyr, 1969, 1995). The accuracy of such ozonesondes is reported to be about ±5-10 % up to ~30 km (Smit et al., 2007). More details of this measurement technique can be found in Ojha et al. (2014).

The accumulated rainfall for every 3-hour interval from the Tropical Rainfall Measuring Mission (TRMM; with a horizontal grid size of 0.25° × 0.25°) is also utilized in this study to complement the onboard rainfall measurements. The 3B42 algorithm is used to calculate precipitation and root-mean-square precipitation-error estimates; these two estimates were then used to compute hourly and daily rainfall estimates (Huffman et al., 1995).

The gridded (2° × 2°) monthly column averaged CH_4 (level-3, version 6) retrievals from SCIAMACHY (SCanning Imaging Absorption spectroMeter for Atmospheric CartograpHY) instrument on board Envisat spacecraft were used to infer concentrations over Indian land regions. The IMAP-DOAS (Iterative maximum a posteriori - differential optical absorption spectroscopy) algorithm was used which retrieves CH_4 utilising the spectra (i.e., 1000–1750 nm) from the near infrared channel#6 (Frankenberg et al., 2005).

4. Model Simulations

The Weather Research and Forecasting model with Chemistry (WRF-Chem; Grell et al., 2005) version-3.5.1 was used to simulate meteorological and chemical fields during the campaign period. The model domain (Fig. 2d-e) is defined on the Mercator projection, centred at 80° E, 15.5° N, at a spatial resolution of 15 km x 15 km. The model has 51 vertical levels from surface to 10 hPa. The simulations were conducted for the period of June 29 to August 31, 2009, covering the complete measurement period. The meteorological inputs have been adopted from ERA-interim reanalyses by the ECMWF. Horizontal winds, temperature, and water vapour are nudged above the planetary boundary layer using a nudging coefficient of 0.0003 s^{-1} (Kumar et al., 2015), employing the Four Dimensional Data Assimilation (FDDA) technique. Anthropogenic emissions of CO, NO_x, SO_2, and NMVOCs are provided by a regional emission inventory that was developed to support the Intercontinental Chemical Transport Experiment – Phase B (INTEX-B; Zhang et al., 2009; Kumar et al., 2012b; Ojha et al., 2016). This inventory is representative of the year 2006. Aerosol emissions are provided by the Hemispheric Transport of Air Pollution (HTAP v2) inventory (Janssens-Maenhout et al., 2015). Biomass burning emissions from NCAR Fire Inventory (FINN; Wiedinmyer et al., 2011), and biogenic emissions calculated online using MEGAN (Guenther et al., 2006) were used in the simulations.

Gas-phase chemistry in the model is represented by the second-generation Regional Acid Deposition Model (RADM2; Stockwell et al., 1990), and the aerosol module is based on MADE SORGAM (Binkowski and Shankar, 1995; Ackermann et al., 1998; Schell et al., 2001). Initial and boundary conditions for chemical fields are provided by the MOZART-4/GEOS5 data. The options used to parameterize different atmospheric processes are given in Table 1. For more information about meteorological nudging, chemical mechanisms, emissions, boundary conditions, and evaluation of WRF-Chem against in situ measurements and satellite data over the Indian region, please see, for example, Kumar et al. (2012a; 2012b; 2015), Ansari et al. (2016), and Ojha et al. (2016). Model-simulated mean spatial distributions of O_3 and CO over the model domain during the study period are shown in Figure 2d-e.

5. Results and Discussion

5.1 Variations in O_3, CO, and CH_4 over the BoB

Figure 2a-c shows the observed variations in O_3, CO, and CH_4 along the ship track during the July 16 to August 17, 2009. The mixing ratios of trace gases show large spatio-temporal variations over the BoB. Levels of O_3 and CO varied in the ranges of 8–54 nmol mol^{-1} (average of 29.7±6.8 nmol mol^{-1}) and 50–200 $nmolmol^{-1}$ (average of 96±25 nmol mol^{-1}), respectively. As CO mixing ratios below the detection limit of the instrument are discarded from the

analysis, the reported minimum and average values of CO mixing ratios are therefore slightly higher than their actual values. CH_4 mixing ratios are observed to range from 1.57–2.15 µmol mol^{-1}, with average of 1.83±0.14 nmol mol^{-1}. Average CH_4 mixing ratios, showed a significant difference of ~0.14 µmol mol^{-1} between northern (81-91° E, 16-21.5° N) and central (80-91° E, 11-16° N) BoB during the study period. In addition to sailing across the BoB, the ship was also kept stationary for fifteen days, from July 22 to August 06, 2009 at 89° E, 19° N. During this time period, surface O_3, CO, and CH_4 mixing ratios are observed to fall into the range of 9–46 nmol mol^{-1}, 58–144 nmol mol^{-1}, and 1.71–1.89 µmol mol^{-1}, respectively, with temporally averaged mixing ratios of 28±7 nmol mol^{-1}, 91±19 nmol mol^{-1}, and 1.81±0.06 µmol mol^{-1}, respectively.

The HYbrid Single Particle Lagrangian Integrated Trajectory (HYSPLIT) model was used to simulate five-day backward airmass trajectories arriving at 500 m (a height that falls within the marine atmospheric boundary layer) above the measurement locations (Draxler and Rolph, 2003; Rolph, 2003; http://www.arl.noaa.gov/ready.html), as shown in the Fig. 3. Trajectories are colour-coded to show the altitude variations of the air parcels along their path. The influences of two different airmasses are observed over the BoB during the CTCZ experiment. Over the central BoB, the backward air trajectories cross southern India (i.e. <13° N), where a belt of elevated anthropogenic emissions (5–20 mol km^{-2} hr^{-1} of NO_x; see Fig. 1) is located. In contrast, most of the air trajectories over northern BoB come across the central Indian region, where anthropogenic emissions are relatively lower. For example, with the exception of a few hotspots, NO_x emissions north of 13° N are in the range of 1–10 mol km^{-2} hr^{-1} (Fig. 1). The O_3 and CO mixing ratios over BoB in airmasses from central/northern India (Fig. 3a) are slightly higher or comparable (O_3: 30±7 nmol mol^{-1}, CO: 95±25 nmol mol^{-1}) to those (O_3: 27±5 nmol mol^{-1}, CO: 101±27 nmol mol^{-1}) in airmasses from southern India (Fig. 3b).

The observed spatio-temporal variations of trace gases are investigated by calculating the fractional residence time of airmasses over land, using HYSPLIT simulated 5-day backward air trajectories. Figure 4a–c shows the temporal variations of O_3, CO, and CH_4 during the CTCZ experiment along the cruise track. The percentage of time of airmasses over continental India is also shown (Fig. 4d), as estimated by the ratio of residence time over land to the total trajectory time of 5 days. The hours of residence have only been included in the analysis if the altitude along trajectory is less than 1.5 km, as the surface emissions might not been directly influence the airmasses aloft. Red vertical bars depict the sharp reductions in O_3 mixing ratios associated with rainfall events (see Section 5.3). O_3, CO and CH_4 show correlated variability with the estimated residence times over the Indian subcontinent with slightly higher correlation in the case of primary species (R^2 = 0.16 in case of CO and CH_4), as compared to O_3 (R^2 = 0.09). Similar variations in mixing ratios of these trace gases and residence time over continental India indicate the influences of transport from the Indian subcontinent on the observed spatio-temporal variations over the BoB during the summer monsoon season. The occasions on which such a one-to-one correspondence are not observed can be attributed to varying source strengths, vertical mixing or dilution, and en route photochemistry.

Generally, during the summer monsoon season, relatively cleaner marine airmasses from the Arabian Sea are transported to the Indian region. These airmasses are then exposed to regional emissions and subjected to photochemistry depending upon the availability of solar insolation under the cloudy conditions of monsoon. The airmasses in which precursors have accumulated, and to some extent photo-chemically processed, outflows into the

BoB. As a result, the airmasses out-flowing at the eastern coast of India could have higher O_3 mixing ratios than the background air coming from the Arabian Sea into the western coast of India. The difference between these two values is representative of the O_3 build-up that can be attributed to regional pollution; this difference would also reflect the extent of photochemical processing that would have taken place.

As the observational site Thumba, Thiruvananthapuram, is situated just at the Arabian Sea coast, the monsoon-time observations here could be approximated to represent the background O_3 mixing ratios entering from the Arabian Sea. In August 2009, using only daytime monthly average O_3, the O_3 at Thumba during the monsoon season was observed to be 23±7 nmol mol^{-1}. Since the objective of investigation is the additional O_3 over the BoB produced by en route photochemistry, daytime O_3 values at Thiruvananthapuram are therefore compared with all the observations over the BoB. The average mixing ratio observed over the BoB during monsoon season for July 16–August 17, 2009 was 30±7 nmol mol^{-1}, which was ~7 nmol mol^{-1} higher than the Arabian Sea airmass. This additional amount of ~7 nmol mol^{-1} could be attributed to the effects of regional and en route photochemical O_3 production. Net O_3 production rate in the outflow is estimated to be in the range of 1.5–4 nmol mol^{-1} day^{-1}. Note that the O_3 mixing ratio is reported to be ~30±2 nmol mol^{-1} during July 2009 over Ananthapur, a rural site in central India, indicating the enhancement due to regional O_3 production. As shown in Table 2, while average O_3 mixing ratios over the west coast of India and the Arabian Sea are in the range of 9–25 nmol mol^{-1} during the monsoon season, the average O_3 mixing ratio is ~ 30 nmol mol^{-1} over the central Indian station and the BoB.

O_3 mixing ratios were 27±3 and 28±5 nmol mol^{-1} for July 21, 2009 and August 15, 2009, for which back-trajectories (not shown here) crossed Thiruvananthapuram on July 20, 2009 and August 13, 2009, with daytime O_3 values of 23±6 and 25±6 nmol mol^{-1}, respectively. The difference of 3–4 nmol mol^{-1} between O_3 mixing ratios over the BoB and Thurivannthapuram represents the en route photochemical production of O_3 in the airmasses toward the observation points over the BoB. It is further found that the airmasses were typically below 700 meters, and generally within the marine boundary layer (e.g. mean boundary layer height ~897 m during winter over the BoB; Subrahamanyam et al., 2012). The enhancements in O_3 are attributed here to in situ photochemical build-up while moving towards the BoB, which has been noted in previous experiments and model simulations (e.g. Lal and Lawrence, 2001; Ojha et al., 2012).

CO showed a sharp enhancement (denoted with red arrows in Fig. 4b) on August 7 and 11, 2009, coinciding with a longer residence time over the Indian region. Figure 5 shows backward airmass trajectories above the measurement locations, along with the distribution of anthropogenic CO emissions from the INTEX-B inventory, representative of the year 2006. The airmasses over the BoB are found to be influenced by emission hotspots (corresponding emission of 250–350 mol km^{-2} hr^{-1}). The airmasses took about half a day to be transported from the emission hotspot to the observation location over the BoB. CO mixing ratios measured at Bhubaneswar (20.30° N; 85.83° E), a station within the hotspot region, is ~251±58 nmol mol^{-1} during the monsoon season (June–August 2011–2012; Mahapatra et al., 2014), with the elevated CO emissions in the Bhubaneswar region being attributed to industrial activities. The higher CO mixing ratios ~200 nmol mol^{-1} is inline with the monsoonal values observaed at Bhubaneswar. The CO mixing ratios around 150 nmol mol^{-1} were sampled on August 11, 2009 near the coastal source regions. Additionally, CO mixing ratios over central BoB (101 nmol mol^{-1}) were only slightly higher than those over

northern BoB (95 nmol mol^{-1}). It is suggested that this is partially due to higher emissions over southern India, against the shorter residence of airmasses over land and the relatively longer lifetime of CO.

The mixing ratios of surface CH_4 were higher in the airmasses from central/northen Indian over northern BoB (1.86±0.12 µmol mol^{-1}) as compared to those in the airmasses from southern India (1.72±0.14 µmol mol^{-1}). As CH_4 is a relatively well mixed trace gas, the average values over the tropospheric column approximates the uniform mixing ratio within the troposphere (Seinfeld and Pandis, 2006). The monthly column averaged tropospheric CH_4, retrievals from SCIAMACHY, for August 2009 shows (Fig. 6) higher values around 1.85 µmol mol^{-1} over central/northern India as compared to that of southern India (~1.80 µmol mol^{-1}). The higher tropospheric CH_4 over the central/northern Indian landmass during the summer monsoon season has been also reported by Kavitha and Nair, 2016. The observed higher CH_4 over the northern BoB are attributed to the influences of emissions from central/northern Indian regions as also suggested by backward trajectories. Owing to the longer lifetime of CH_4, diffusion of CH_4 from a hotspot region over the eastern IGP to northern BoB might be the other source of higher CH_4 levels over northern BoB during summer monsoon season. An emission inventory analysis by sector over the hotspot region (i.e. eastern IGP) indicates that these higher CH_4 emissions are associated with rice cultivation, waste treatment and livestock. The correlation between the in situ CH_4 measurements and the retrievals from the satellite instrument (AIRS–Atmospheric Infrared Sounder) was found to be statistically insignificant (not shown) which highlights a need of more such in situ measurements in this region to validate the satellite products especially during the summer monsoon.

5.2 WRF-Chem simulations

WRF-Chem simulations, as described in Section 4, are used to evaluate the performance of the model in reproducing the measurements, and to investigate the underlying processes that caused the observed variabilities in O_3 and CO. A comparison between model simulated and measured meteorological parameters shows only small mean biases, such as -1.9 hPa in pressure, -0.6° C in temperature, and -1.1% in relative humidity (Table 3). Figure 4b-c compares WRF-Chem-simulated O_3 and CO with in situ measurements taken along the cruise track. WRF-Chem is found to reproduce the observed variations of O_3 and CO over the BoB during the summer monsoon season with an overestimation of absolute O_3 levels by 1.9 nmol mol^{-1} (i.e. ~6% of averaged O_3 value, 29.7 nmol mol^{-1}) and absolute CO levels by 18 nmol mol^{-1} (i.e. ~16% of averaged CO value, 96 nmol mol^{-1}). It should be noted that the average CO mixing ratio of 96 nmol mol^{-1} is slightly higher than its actual value, as data points below the detection limit of the instrument are discarded. Biases in the model simulations can be attributed to the uncertainties in the simulated meteorology and in the emission datasets; however, in the present study, the model fields are used mainly to investigate temporal variations rather than absolute mixing ratios. The squared correlation coefficients between the daily averaged in situ measured and simulated O_3 and CO are 0.58 and 0.19, respectively. The higher value of the squared correlation coefficient for O_3 demonstrates WRF-Chem's ability to reproduce the observed broad features in surface O_3 over the BoB. Note that the sharp reductions that caused very low O_3 during rainfall episodes are not captured by WRF-Chem, except during the event of August 10–11, 2009. This will be discussed in detail in Section 5.3. WRF-Chem simulated O_3 has also been evaluated against several surface observations in India

previously (Kumar et al., 2012b). Modeled O_3 was found to be within 1-σ standard deviation of mean from observations at Gadanki in the southern India during summer monsoon (Ojha et al., 2016). At Thumba also, model simulated O_3 variations correlated reasonably with measurements (R^2=0.6). More information on evaluation of WRF-Chem simulations of O_3 and CO over India can be found elsewhere (e. g. Kumar et al., 2012b; Ojha et al., 2016).

An additional simulation was conducted by switching off the anthropogenic emissions over the model domain (Fig. 4b-c; dotted blue curves). Mean O_3 (17.7 nmol mol^{-1}) is found to be lower by 14 nmol mol^{-1} with smaller variability of 2.4 nmol mol^{-1} compared to standard WRF-Chem simulation. Similarly, also the mean CO level is lower by 36 nmol mol^{-1} with smaller variability of 4.9 nmol mol^{-1}. This shows that enhanced levels and observed variability in O_3 and CO mixing ratios over BoB are attributable to the regional anthropogenic emissions.

The limited collocated measurements showed en route O_3 production rate of 1.5–4 nmol mol^{-1} day^{-1}, as discussed in section 5.2. Here, the O_3 production rate is estimated by analyzing the model simulated O_3 mixing ratios along the airmass trajectories ending at few representative locations over the BoB (Fig. 7a). The model simulated chemical evolution of air parcels clearly shows an increase in the O_3 mixing ratios towards the marine region of BoB. The temporal variations of O_3 mixing ratio averaged corresponding all the trajectories shown in Fig. 7a is shown as a boxplot in Fig. 7b. A linear regression analysis (blue curve in Fig. 7b), is used to estimate the mean en route O_3 production rate of ~4.6 nmol mol^{-1} day^{-1} in the outflow. The enhancement in average O_3 over the BoB as compared to the continental Indian region is also shown in the Fig. 2d, averaged for the study period.

5.3 Ozone variations during rainfall events

An interesting phenomenon observed during the CTCZ experiment is the abrupt reduction in O_3 mixing ratios that accompanied the onset of heavy rainfall, despite the low solubility of O_3 in water. In this section the possible causes of these low-O_3 events during rainfall are investigated.

Figure 8 shows variations in O_3 (black circles) mixing ratios, surface temperature (orange curve), TRMM-retrieved rainfall (thick grey vertical bars), and WRF-Chem-simulated vertical winds at pressure levels ranging from 950–750 hPa (coloured bars) during four such events on July 21, 26, and 28–29 and on August 10–11, 2009. As high time-resolution in situ measurements of rainfall were not available aboard ship, Figure 8 therefore uses 3-hourly rainfall retrievals from the TRMM, co-located with O_3 measurements. During these events, CO mixing ratios also show a reduction of about ~56 nmol mol^{-1}, with observed values falling below the detection limit of the instrument during the first event of July 21, 2009 (not shown). Although CO measurements are not available for the second and third event, during the fourth event (August 10–11, 2009) CO mixing ratios showed an enhancement due to transport from strong source regions (see Section 5.1). While the first three low-O_3 events are not captured by WRF-Chem (Fig. 4c), the fourth event is reproduced.

Wet scavenging does not directly reduce O_3, as its water solubility is low; as a result, some dynamic process could be responsible for the observed reductions in O_3 during rainfall. Airmasses could undergo downdrafts during heavy rainfall (Kumar et al., 2005) through air drag by the falling rain drops and in mesoscale subsidence that compensates convective updrafts. We suggest that, in the presence of O_3-poor airmass aloft, a downdraft would result in

reductions in surface O_3 mixing ratios. An opposite scenario leading to O_3 enhancement could take place if downdrafts bring mid-troposheric air, where typically O_3 is higher than at surface. The model-simulated meteorology shows occurrences of downdrafts at different pressure levels during the first three events on July 21, 26, and 28–29 (Fig. 8a–c), which is further corroborated with measurements of air temperature aboard. Downdrafts of free tropospheric air could lead to a reduction in near-surface temperature by as much as 10 °C within a few minutes (Ahrens, 2009). Air temperature measured aboard ship showed a sharp decrease of 2–4 °C, coinciding with the first three low-O_3 events (Fig. 8a-c). The reductions in temperature caused by downdrafts are generally short-lived (Ahrens, 2009), it is confirmed in the case of these events (Fig. 8a-c).

Model-simulated vertical winds and variations in air temperature suggest that downdrafts did occur during the first three rainfall events. As in situ measurements of O_3 vertical profiles are not available over the BoB during the summer monsoon season, the observations taken at Thumba, Thiruvananthapuram, in the southern Indian region are used as a case study to investigate this hypothesis. For general details of the typical diurnal and seasonal variations of O_3 at Thumba, please see Nair et al. (2002), David and Nair (2011), and Girach et al. (2012). Figure 9a shows the temporal variation in surface O_3 on July 15, 2011 at Thumba, along with 5-minute accumulated rainfall. Here, surface O_3 is observed to decline from 25 to 13 nmol mol^{-1} within 15–20 minutes, coinciding with the occurrence of intense rainfall (3.5–0.5 mm rain over a period of 5 minutes). Measurements of the O_3 vertical profile are not available for this day due to the rainy conditions; a profile measured on July 28, 2011 is therefore shown in Fig. 9b. This profile has lower O_3 mixing ratios aloft (~22 nmol mol^{-1} at ~1 km) than near surface (~42 nmol mol^{-1}). The observed mixed layer height is about 0.15–0.6 km over Thumba, Thiruvananthapuram (Anurose et al., 2016) during July 2011; above this height, O_3 mixing ratios sharply decrease with altitude. The present case study suggests the presence of O_3-poor airmasses aloft than those near the surface over the south Indian region during summer monsoon. With an O_3 distribution as observed in the present case study at Thumba, the downdraft during intense rainfall could lead to the mixing of free-tropospheric air with near-surface air, or to the replacement of surface air with free-tropospheric O_3-poor air.

Although air temperature measurements could not be made during the fourth event (10–11 August 2009) due to a technical problem, model meteorology does not indicate a downdraft during this event (Fig. 8d), indicating the dominance of a different process. As WRF-Chem-simulated O_3 variability is in good agreement with observations during this event, various tendency terms (Barth et al., 2012) from WRF-Chem are used to investigate the relative influences of different processes. The variations in instantaneous values for horizontal advection tendency, vertical advection tendency, and net tendency (i.e. the sum of chemical, vertical mixing, convective, vertical advection, and horizontal advection), along with modelled O_3 over the two locations during the event are shown in Figure 10. The tendency values shown here are derived by subtracting the accumulated tendencies at $(n-1)^{th}$ hour from the accumulated tendency at n^{th} hour. The vertical dotted lines show the time of a low-O_3 event.

Both the horizontal and net tendencies (Fig. 10b-c,e-f) show negative values, indicating that they are contributing towards a reduction in O_3 mixing ratios (Fig. 10a,d). However, as the time of the event approaches, it is the horizontal advection tendency term that is significantly negative (Fig. 10c, f), while other terms are small and close to zero. Horizontal advection is therefore suggested to dominate during the low-O_3 event of August 10–11, 2009.

The influence of horizontal advection on O_3 during this event is shown more clearly in Fig. 11, which shows the spatial distribution of O_3 and CO from WRF-Chem before the event (16:00 and 19:00 UT) and during the event (22:00 UT) on August 10, 2009. The white triangles show the two locations where the event was observed. During 16:00 and 19:00 UT, a patch of high O_3 mixing ratios (35 nmol mol^{-1} and higher) is seen to be distributed over a large region surrounding the measurement location. This large patch of elevated O_3 mixing ratios is horizontally advected eastward from 16:00 to 19:00 and then towards 22:00 UT (event time). As a result of this rapid advection, the high-O_3 airmasses are transported from the coastal regions to deeper into the BoB; by the time they reached the location of observation, O_3 mixing ratios are observed to be lower (25–35 nmol mol^{-1}) during the event time (22:00 UT). A patch of higher levels of CO (~300 nmol mol^{-1}) was also found to be distributed across the east coast of the Indian region. Transport and dilution of this CO patch is, however, less pronounced than the high-O_3 airmasses, possibly due to the relatively longer lifetime of CO. Thus, in nutshell, the horizontal advection played a key role in transporting O_3-rich airmasses deeper into the BoB region, while it diluted O_3 levels near the coastal regions in southern India during the fourth event.

5.4 Seasonal variation in trace gases over the BoB

In this section, the monsoon-time measurements of O_3 taken in the present study are combined with data from previous campaigns (see Table 4) to investigate the seasonal variation in O_3 over the BoB (Fig. 12). O_3, CO, and CH_4 mixing ratios are averaged over northern (81-91° E, 16-21.5° N) and central (80-91° E, 11-16° N) BoB regions. Overall, higher O_3 mixing ratios are present over both northern and central BoB during the winter, while lower O_3 levels are observed during the spring–summer (with more scatter in the data over central BoB). The O_3 seasonal amplitude (i.e., the range from maxima to minima) is estimated to be ~ 39 nmol mol^{-1} over northern BoB and ~ 27 nmol mol^{-1} over central BoB. The monsoonal surface O_3 mixing ratios (~30±7 nmol mol^{-1}) are nearly half those observed during winter (63±5 nmol mol^{-1}) over northern BoB. During December 2008–January 2009, February 2003, March 2006, and November 2010, the O_3 mixing ratios were higher (by ~3–22 nmol mol^{-1}) over northern BoB than those over central BoB. However, over the course of February 2001, O_3 mixing ratios were higher over central BoB (~38 nmol mol^{-1}) than that over northern BoB (~14 nmol mol^{-1}). In contrast, during summer monsoon season, average O_3 mixing ratios are comparable or only slightly higher over northern BoB (30±7 nmol mol^{-1}) as compared to that over central BoB (27±5 nmol mol^{-1}).

As compared with the summer monsoon season, when CO mixing ratios were lower, over northern BoB, CO mixing ratios were higher during the winter, while over central BoB, CO mixing ratios were higher during the pre-monsoon season. For O_3, spring–summer had the lower mixing ratios in both regions. The seasonal amplitude in CO mixing ratios is estimated to be ~205 nmol mol^{-1} over northern BoB and ~124 nmol mol^{-1} over central BoB. The monsoonal CO mixing ratio (~95 nmol mol^{-1}) is about one third that of the winter season (302 nmol mol^{-1}) over northern BoB. During the present study, average CO mixing ratios were comparable over northern (95±25 nmol mol^{-1}) and central BoB (101±27 nmol mol^{-1}).

A clear inference about seasonal patterns is difficult in the case of CH_4, however a tendency of lower levels towards winter can be seen. Higher mixing ratios ~1.95 (~1.91) µmol mol^{-1} were observed during November 2010 over

northern BoB, and during February–March 2001 over central BoB, as compared to those from other studies. The surface CH_4 observations obtained during the present study show the highest variability (i.e. the difference between maxima and minima) when compared to earlier studies: 0.53 μmol mol^{-1} over northern BoB and 0.39 μmol mol^{-1} over central BoB. This high variability is attributed to the relative source strengths over central and northern India as compared to southern India, highlighting the regional differences in CH_4 variability across India (Kavitha and Nair, 2016).

Seasonal variations in trace gases over the BoB are attributed to seasonal changes in the meteorological conditions, emissions, and photochemistry over the South Asian region, as well as to synoptic scale transport patterns. Wintertime stronger westerly winds transport the pollution from South Asia including that of the Indo-Gangetic basin to the BoB region. Monsoonal circulation, in contrast, carries cleaner marine airmasses to the BoB from the oceanic regions. However, as observed during the CTCZ, polluted continental or coastal airmasses can also occasionally be transported deeper over the BoB. Intense monsoonal rainfall generally leads to wet removal of O_3 precursors, while cloudy and rainy meteorological conditions suppress O_3 formation. Along with the importance of monsoonal convection in cloud formation, rainfall, and uplifting the boundary layer pollution, rapid horizontal advection is also an important process during the summer monsoon, especially affecting the near-surface variability of trace gases over the oceanic regions adjacent to India.

6. Conclusions

In this paper, we presented ship-borne in situ measurements of O_3, CO, and CH_4 that were carried out as a part of the CTCZ experiment over the BoB during the summer monsoon season, July–August 2009. We analyzed the spatial and temporal variations in the observations and compared them with results from simulations performed with a regional chemistry transport model (WRF-Chem), as well as with observations from previous campaigns over the BoB. The main conclusions are:

1. These first monsoonal observations of O_3, CO, and CH_4 show large spatio-temporal variability over the BoB, with mixing ratios varying in the range of 8–54 (mean: 29.7±6.8) nmol mol^{-1}, 50–200 (mean: 96±25) nmol mol^{-1}, and 1.57–2.15 (mean: 1.83±0.14) μmol mol^{-1}, respectively. The O_3 and CO mixing ratios in airmasses from central/northern India are slightly higher or comparable (O_3: 30±7 nmol mol^{-1}, CO: 95±25 nmol mol^{-1}) to those in airmasses from southern India (O_3: 27±5 nmol mol^{-1}, CO: 101±27 nmol mol^{-1}). The CH_4 mixing ratios in airmasses from central/northern (1.86±0.12 μmol mol^{-1}) are higher (~0.14 μmol mol^{-1}) compared to those in airmasses from southern India (1.72±0.14 μmol mol^{-1}). This could be due to higher CH_4 levels over central/northern India, also found in SCIAMACHY data.
2. Back-trajectory analysis shows effects of long-range transport from northern or central India to northern BoB, and from southern India to central BoB. The correlated variations of these trace gases and percentage residence time of air parcels over the Indian regions suggest that the enrichment of O_3 and precursors in air parcels over the BoB is associated with both emissions and photochemistry over the Indian region. The trajectory analysis show that the observed variation in surface O_3 is primarily due to transport and en route photochemistry over the BoB

during monsoon season. An analysis of modeled O_3 along airmass trajectories show mean en route O_3 production rate of about 4.6 nmol mol^{-1} day^{-1} in the outflow towards the BoB.

3. The observed spatio-temporal variations of surface O_3 and CO during summer monsoon season are generally reproduced by the WRF-Chem model, although the absolute mixing ratios of O_3 and CO are typically overestimated by about 6 and 16 % respectively.
4. The four low-O_3 events coinciding with intense rainfall were observed over the BoB. After analysing the observed variability in air temperature, model simulations of vertical winds, and an O_3-profile case study from southern India, we suggest that first three low-O_3 events were due to strong downdrafts of O_3-poor airmasses. Analysis of the fourth event, which is successfully reproduced by the model, shows the pivotal role of horizontal advection in transporting O_3-rich airmasses deeper over the BoB.
5. Finally, the measurements during the monsoon are combined with previous campaigns over the BoB during other seasons to investigate the seasonal variability in trace gases over the BoB. O_3 and CO are shown to have pronounced seasonality, O_3 having amplitudes of about 39 and 27 nmol mol^{-1}, and CO having amplitudes of about 207 and 124 nmol mol^{-1} over northern and central BoB, respectively.

Our study data fill a gap of observations during the summer monsoon over the BoB, providing information on the extent of seasonal variability. We recommend supplementing these findings with ship-borne experiments featuring collocated vertical profile observations from balloon-borne and aircraft-based platforms over the oceanic regions surrounding India to better understand the role of both large-scale dynamics (e.g. Ojha et al., 2016) and of regional influences due to South Asian outflow (see Lawrence and Lelieveld, 2010, and references therein). Such a future study would also improve our understanding of the changes that take place in the atmospheric oxidation capacity during the summer monsoon season.

Acknowledgements

We thank the CTCZ and ICRP organizers for the opportunity to participate in the 2009 CTCZ experiment. We are thankful to the Director of the National Centre for Antarctic and Ocean Research (NCAOR), Goa, for providing ship-board facilities. We gratefully acknowledge Prof. G. S. Bhatt (Indian Institute of Science, Bengaluru, India) and his team for providing the measurements of meteorological parameters. We also thank the chief scientist on board *SagarKanya* for providing necessary support during the cruise. The authors gratefully acknowledge the NOAA Air Resources Laboratory (ARL) for the providing the HYSPLIT transport and dispersion model and READY website (http://www.arl.noaa.gov/ready.php) used in this publication. The rainfall estimations (3B42) from the TRMM satellite were obtained from the NASA/GSFC via their website http://mirador.gsfc.nasa.gov/. The monthly CH_4 retrievals (IMAP-DOAS) of SCIAMACHY were obtained from their website, http://www.temis.nl/climate/methane.html. Use of INTEX-B and HTAP (http://edgar.jrc.ec.europa.eu/htap_v2/index.php?SECURE=123) anthropogenic emissions is gratefully acknowledged. Initial and boundary-conditions data for meteorological fields were used from the ERA interim of ECMWF. Use of MOZART-4/GEOS5 initial and boundary conditions data for chemical fields is acknowledged. Data/processors for anthropogenic emissions, biogenic emissions, and biomass burning obtained from NCAR ACD

website are gratefully acknowledged. The authors acknowledge the use of MPG supercomputer HYDRA (http://www.mpcdf.mpg.de/services/computing/hydra) for model simulations. Constructive comments and suggestions from anonymous reviewers are gratefully acknowledged.

References

Ackermann, I. J., Hass, H., Memmesheimer, M., Ebel, A., Binkowski, F. S., and Shankar, U.: Modal aerosol dynamics model for Europe: development and first applications, Atmos. Environ., 32, 2981–2999, 1998.

Ahrens, C. D.: Meteorology Today- an introduction to weather, climate, and the environment, Brooks/Cole, USA, 2009.

Ali, K., Beig G., Chate D. M., Momin, G. A., Sahu, S. K., and Safai, P. D.: Sink mechanism for significantly low level of ozone over the Arabian Sea during monsoon, J. Geophys. Res., 114, D17306, doi:10.1029/2008JD011256, 2009.

Ansari, T. U., Ojha, N., Chandrasekar, R., Balaji, C., Singh, N., and Gunthe, S. S.: Competing impact of anthropogenic emissions and meteorology on the distribution of trace gases over Indian region, J. Atmos. Chem., pp. 1-18, doi:10.1007/s10874-016-9331-y, 2016.

Anurose, T. J., Subrahamanyam D. B., Sunilkumar S. V.: Two years observations on the diurnal evolution of coastal atmospheric boundary layer features over Thiruvananthapuram (8.5◦ N, 76.9◦ E), India, Theor Appl Climatol, doi: 10.1007/s00704-016-1955-y, 2016.

Barth, M. C., Lee, J., Hodzic, A., Pfister, G., Skamarock, W. C., Worden, J., Wong, J., and Noone D.: Thunderstorms and upper troposphere chemistry during the early stages of the 2006 North American Monsoon, Atmos. Chem. Phys., 12, 11,003–11,026, doi:10.5194/acp-12-11003-2012, 2012.

Bergamaschi, P., Hein, R., Heimann, M., and Crutzen, P. J.: Inverse modeling of the global CO cycle: 1. Inversion of CO mixing ratios, J. Geophys. Res.-Atmos., 105, 1909–1927, doi:10.1029/1999JD900818, 2000.

Binkowski, F. S. and Shankar, U.: The regional particulate matter model: 1. Model description and preliminary results, J. Geophys. Res., 100, 26191–26209, doi:10.1029/95JD02093, 1995.

Brasseur, G. P., Orlando, J. J., and Tyndall, G. S.: Atmospheric Chemistry and Global Change. Oxford University Press, New York, pp. 209-234, 1999.

Chen, F. and Dudhia, J.: Coupling and advanced land surface-hydrology model with the Penn State-NCAR MM5 modeling system, Part I: Model implementation and sensitivity, Mon. Weather Rev., 129, 569–585, 2001.

Chou, M.-D. and Suarez, M. J.: An effcient thermal infrared radiation parametrization for use in general circulation models, NASA Tech. Memo., 104606, 85 pp., 1994.

Cooper, O. R., Parrish, D. D., Ziemke, J., Balashov, N. V.,Cupeiro, M., Galbally, I. E., Gilge, S., Horowitz, L. , Jensen, N. R., Lamarque, J.-F., Naik, V., Oltmans, S. J., Schwab, J., Shindell, D. T., Thompson, A. M., Thouret, V., Wang, Y., and Zbinden, R. M.: Global distribution and trends of tropospheric ozone: An observation-based review, Elementa: Science of the Anthropocene,2: 000029,doi: 10.12952/journal.elementa.000029, 2014.

Crutzen, P. J., Lawrence, M. G., and Poschl, U.: On the background photochemistry of tropospheric ozone.Tellus 51A, 123-146, 1999.

David, L. M. and Nair, P. R.: Diurnal and seasonal variability of surface ozone and NOx at a tropical coastal site: Association with mesoscale and synoptic meteorological conditions, J. Geophys. Res., 116, D10303, doi:10.1029/2010JD015076, 2011.

David, L. M., Girach, I. A., Nair, P. R.: Distribution of ozone and its precursors over Bay of Bengal during winter 2009: role of meteorology, Ann. Geophys., 29, 1613–1627, doi:10.5194/angeo-29-1613-2011, 2011.

Draxler, R. R. and Rolph, G. D.: HYSPLIT (HYbrid Single-Particle Lagrangian Integrated Trajectory) Model access via NOAA ARL READY Website (http://www.arl.noaa.gov/HYSPLIT.php), NOAA Air Resources Laboratory, Silver Spring, MD, 2003.

Finlayson-Pitts, B. J., and Pitts Jr., J. N.: Chemistry of the Upper and Lower Atmosphere: Theory, Experiments, and Applications. Academic Press, USA, 2003.

Fishman, J., Solomon, S., and Crutzen, P. J.: Observational and theoretical evidence in support of a significant in situ photochemical source of tropospheric ozone, Tellus, 31, 432–446, 1979.

Frankenberg, C., Platt, U., and Wagner T.: Iterative maximum a posteriori (IMAP)-DOAS for retrieval of strongly absorbing trace gases: Model studies for CH_4 and CO_2 retrieval from near infrared spectra of SCIAMACHY onboard ENVISAT, Atmos. Chem. Phys., 5, 9–22, 1680-7324/acp/2005-5-9, 2005.

Fung, I., John, J., Lerner, J., Matthews, E., Prather, M., Steele, L. P., and Fraser, P. J.: Three-dimensional model synthesis of the global methane cycle, J. Geophys. Res. 96, 13033-13065, 1991.

Girach, I.A. and Nair, P.R.: Spatial distribution of near-surface CO over bay of Bengal during winter: role of transport. J. Atmos. Solar Terr. Phys., 72, 1241–1250, doi:10.1016/j.jastp.2010.07.02, 2010.

Girach, I. A., P. R. Nair, L. M. David, P. Hegde, M. K. Mishra, G. M. Kumar, S. M. Das, N. Ojha, and Naja M.: The changes in near-surface ozone and precursors at two nearby tropical sites during annular solar eclipse of 15 January 2010, J. Geophys. Res., 117, D01303, doi:10.1029/2011JD016521, 2012.

Grell, G. A., Peckham, S. E., Schmitz, R., McKeen, S. A., Frost, G., Skamarock, W. C., and Eder, B.: Fully coupled "online" chemistrywithin the WRF model, Atmos. Environ., 39, 6957–6975, 2005.

Grell, G.A. and D. Devenyi, 2002: A generalized approach to parameterizing convection combining ensemble and data assimilation techniques, Geophysical Research Letters, 29, 14, doi:10.1029/2002GL015311, 2002.

Guenther, A., Karl, T., Harley, P., Wiedinmyer, C., Palmer, P. I., and Geron, C.: Estimates of global terrestrial isoprene emissions using MEGAN (Model of Emissions of Gases and Aerosols from Nature), Atmos. Chem. Phys., 6, 3181–3210, doi:10.5194/acp-6-3181-2006, 2006.

Heagle, A.S.: Ozone and crop yield. Annual Review of Phytopathology 27, 397-423, 1989.

Huffman, G. J., Adler, R. F., Rudolf, B., Schneider, U., and Keehn, P. R.:Global precipitation estimates based on a technique for combining satellite-based estimates, rain gauge analysis, and NWP model precipitation information. J. Clim. 8, 1284-1295,doi: 10.1175/1520-0442(1995)008<1284:GPEBOA>2.0.CO; 2, 1995.

IPCC-AR5, Fifth Assessment Report of the Intergovernmental Panel on Climate Change, 2013.

Jacob, D.: Introduction to Atmospheric Chemistry, Princeton University Press, 1999.

Janjic, Z. I.: The surface layer in the NCEP Eta Model, Eleventh Conference on Numerical Weather Prediction, Norfolk, VA, 19–23 August, Amer. Meteor. Soc., Boston, Boston, MA, 354–355, 1996.

Janjic, Z. I.: Nonsingular Implementation of the Mellor-Yamada Level 2.5 Scheme in the NCEP Meso Model, NCEP office Note, 437, 61 pp., 2002.

Janssens-Maenhout, G. Crippa, M. Guizzardi, D. Dentener, F. Muntean, M. Pouliot, G. Keating, T. Zhang, Q. Kurokawa, J. Wankmuller, R. Denier van der Gon, H. Klimont, Z. Frost, G. Darras, S. and Koffi, B.: HTAP_v2: a mosaic of regional and global emission gridmaps for 2008 and 2010 to study hemispheric transport of air pollution, Atmos. Chem. Phys. Discuss., 15, 12867-12909, doi:10.5194/acpd-15-12867-2015, 2015.

Kavitha, M. and Nair P. R.:Region-dependent seasonal pattern of methane over Indian region asobserved by SCIAMACHY,Atmospheric Environment 131, 316-325, doi: 10.1016/j.atmosenv.2016.02.008, 2016.

Komhyr, W. D.: Electrochemical concentration cells for gas analysis, Ann. Geophys. 25, 203-210,1969.

Komhyr, W. D., Barnes, R. A., Brothers, G. B., Lathrop, J. A., and Opperman, D. P.: Electrochemical concentration cell ozonesonde performance evaluation during STOIC 1989, J. Geophys. Res. 100 (D5), 9231-9244, doi: 10.1029/94JD02175, 1995.

Kumar K. K., Jain A. R., and Rao D. N.: VHF/UHF radar observations of tropical mesoscaleconvectivesystems over southern India, Annales Geophysicae, 23, 1673–1683, 1432-0576/ag/2005-23-1673, 2005.

Kumar, R., M. Naja, G. G. Pfister, M. C. Barth, and Brasseur, G. P.: Simulations over South Asia using the Weather Research and Forecasting model with Chemistry (WRF-Chem): set-up and meteorological evaluation, Geosci. Model. Dev., 5, 321–343, doi:10.5194/gmd-5-321-2012, 2012a.

Kumar, R., Naja, M., Pfister, G. G., Barth, M. C., Wiedinmyer, C., and Brasseur, G. P.: Simulations over South Asia using theWeather Research and Forecasting model with Chemistry (WRFChem): chemistry evaluation and initial results, Geosci. ModelDev., 5, 619–648, doi:10.5194/gmd-5-619-2012, 2012b.

Kumar, R., M. C. Barth, G. G. Pfister, V. S. Nair, S. D. Ghude, and Ojha N.: What controls the seasonal cycle of black carbon aerosols in India?, J. Geophys. Res. Atmos., 120, doi:10.1002/2015JD023298, 2015.

Lal, S., Chand, D., Sahu, L.K., Venkataramani, S., Brasseur, G., Schultz, M.G.:High levels of ozone and related gases over the Bay of Bengal during winter and early spring of 2001, Atmos. Environ. 40, 1633-1644, 2006.

Lal, S. and Lawrence, M. G.: Elevated mixing ratios of surface ozone over the Arabian Sea, Geophysical Research Letters 28, 1487-1490, 2001.

Lal, S., Naja, M., and Subbaraya, B.H.: Seasonal variations in surface ozone and its precursors over an urban site in India, Atmos. Environ., 34(17), 2713–2724, doi:10.1016/S1352-2310(99)00510-5, 2000.Lal, S., Sahu, L.K., and Venkataramani, S.: Impact of transport from the surrounding continental regions on the distributions of ozone and related trace gases over the Bay of Bengal during February 2003, J. Geophys. Res. 112, D14302, doi:10.1029/2006JD008023, 2007.

Lawrence, M. G., and J. Lelieveld: Atmospheric pollutant outflow from southern Asia: a review, Atmos. Chem. Phys., 10, 11017–11096, doi:10.5194/acp-10-11017-2010, 2010.

Lelieveld, J., and F. J. Dentener: What controls tropospheric ozone?, J. Geophys.Res., 105, 3531-3551, doi:10.1029/1999JD901011, 2000.

Lelieveld, J., P. J. Crutzen, V. Ramanathan, M. O. Andreae, C. A. M. Brenninkmeijer, T. Campos, G. R. Cass, R. R. Dickerson, H. Fischer, J. A. de Gouw, A. Hansel, A. Jefferson, D. Kley, A. T. J. de Laat, S. Lal, M. G. Lawrence, J. M. Lobert, O. L. Mayol-Bracero, A. P. Mitra, T. Novakov, S. J. Oltmans, K. A. Prather, T. Reiner, H. Rodhe, H. A. Scheeren, D. Sikka, and J. Williams: The Indian Ocean experiment: Widespread air pollution from South and Southeast Asia, Science, 291, 1031–1036, 2001.

Lelieveld, J., H. Berresheim, S. Borrmann, P. J. Crutzen, F. J. Dentener, H. Fischer, J. Feichter, P. J. Flatau, J. Heland, R. Holzinger, R. Korrmann, M. G. Lawrence, Z. Levin, K. M. Markowicz, N. Mihalopoulos, A. Minikin, V. Ramanathan, M. de Reus, G. J. Roelofs, H. A. Scheeren, J. Sciare, H. Schlager, M. Schultz, P. Siegmund, B. Steil, E. G. Stephanou, P. Stier, M. Traub, C. Warneke, J. Williams, H. Ziereis, Science, vol 298, issue 5594, pp. 794-799, doi: 10.1126/science.1075457, 2002.

Lin, Yuh–Lang, R. D., Farley, and H. D., Orville: Bulk Parameterization of the Snow Field in a Cloud Model. J.Climate Appl. Met., 22, 1065–1092, 1983.

Mahapatra, P. S., Panda, S., Walvekar, P. P., Kumar, R., Das, T., and Gurjar, B. R.: Seasonal trends, meteorological impacts, and associated health risks with atmospheric concentrations of gaseous pollutants at an Indian coastal city. Environ SciPollut Res, doi: 10.1007/s11356-014-3078-2, 2014.

Mallik, C., Lal, S., Venkataramani, S., Naja, M., and Ojha, N.: Variability in ozone and its precursors over the Bay of Bengal during post monsoon: Transport and emission effects, J. Geophys. Res. Atmos., 118, doi:10.1002/jgrd.50764, 2013.

Mlawer, E. J., Taubman, S. J., Brown, P. D., Iacono, M. J., and Clough, S. A.: Radiative transfer for inhomogeneous atmospheres: RRTM, a validated correlated-k model for the longwave, J. Geophys. Res.-Atmos., 102, 16663–16682, doi:10.1029/97JD00237, 1997.

Mühle, J., Zahn, A., Brenninkmeijer, C.A.M., Gros, V., and Crutzen, P.J.: Air mass classification during the INDOEX R/V cruise using measurements of non-methane hydrocarbons, CH, CO_2, CO, ^{14}CO, and δ18O(CO), J. Geophys. Res. 107(D19), 8021, doi:10.1029/2001JD000730, 2002.

Monks, P. S., Archibald, A. T., Colette, A., Cooper, O., Coyle, M., Derwent, R., Fowler, D., Granier, C., Law, K. S., Mills, G. E., Stevenson, D. S., Tarasova, O., Thouret, V., von Schneidemesser, E., Sommariva, R., Wild, O., and Williams, M. L.: Tropospheric ozone and its precursors from the urban to the global scale from air quality to short-lived climate forcer, Atmos. Chem. Phys., 15, 8889-8973, doi:10.5194/acp-15-8889-2015, 2015.

Moorthy K. K., V. S. Nair, Babu S. S., and Satheesh S. K.: Spatial and vertical heterogeneities of aerosol radiative forcing over the oceanic regions surrounding the Indian peninsula: climate implications, Q. J. R. Meteorol. Soc., 135, 2131-2145, 2009.

Nair, P. R., Chand, D., Lal, S., Modh, K. S., Naja, M., Parameswaran, K., Ravindran, S., and Venkataramani, S.: Temporal variations in surface ozone at Thumba (8.6 N, 77 E) –a tropical coastal site in India, Atmos. Environ., 36, 603–610, doi:10.1016/S1352-2310(01)00527-1, 2002.

Nair, P. R., David, L. M., Girach, I. A., and George, S. K.: Ozone in the marine boundary layer of Bay of Bengal during post-winter period: Spatial pattern and role of meteorology, Atmos. Environ., 45, 4671–4681, 2011.

Nair, V. S., S. K. Satheesh, K. K. Moorthy, S. S. Babu, S. K. George, and Nair P. R.: Surprising observation of large Anthropogenic Aerosol Fraction over the near-pristine Southern Bay of Bengal: Climate Implications, J. Geophys. Res. Atmos., 115, D21201, doi:10.1029/2010JD013954, 2010.

Naja, M., Lal, S., Chand, D.: Diurnal and seasonal variabilities in surface ozone at a high altitude site Mt Abu (24.6°N, 72.7°E, 1680 m asl) in India. Atmos. Environ. 37, 4205-4215, doi:10.1016/S1352-2310(03)00565-X, 2003.

Naja, M., D. Chand, L. Sahu, and LalS.: Trace gases over marineregions around India, Ind. J. Mar. Sci., 33(1), 95–106, 2004.

Nishanth, T., Praseed, K.M., Satheesh Kumar, M.K., Valsaraj, K.T.: Observational Study of Surface O_3, NO_x, CH_4 and Total NMHCs at Kannur, India, Aerosol and Air Quality Research, 14: 1074–1088, doi: 10.4209/aaqr.2012.11.0323, 2014.

Ojha, N., M. Naja, K. P. Singh, T. Sarangi, R. Kumar, S. Lal,M. G. Lawrence, T. M. Butler, and Chandola H. C.:Variabilities in ozone at a semi-urban site in the Indo-Gangetic Plain region: Association with the meteorology and regional process, J. Geophys. Res., 117, D20301, doi:10.1029/2012JD017716, 2012.

Ojha N., M. Naja, T. Sarangi, R. Kumar, P. Bhardwaj, S. Lal, S. Venkataramani, R. Sagar, A. Kumar, Chandol H.C.: On the processes influencing the vertical distribution of ozone over the central Himalayas: Analysis of yearlong ozonesonde observations, Atmospheric Environment 88, 201-211, doi: 10.1016/j.atmosenv.2014.01.031, 2014.

Ojha, N., Pozzer, A., Rauthe-Schöch, A., Baker, A. K., Yoon, J., Brenninkmeijer, C. A. M., and Lelieveld, J.: Ozone and carbon monoxide over India during the summer monsoon: regional emissions and transport, Atmos. Chem. Phys., 16, 3013-3032, doi:10.5194/acp-16-3013-2016, 2016.

Randel, W. J., Park, M., Emmons, L., Kinnison, D., Bernath, P.,Walker, K. A., Boone, C., and Pumphrey H.: Asian monsoontransport of pollution to the stratosphere, Science, 328, 611–613, 2010.

Ravikumar K., Tiwari Y. K., Valsala V., and Murtugudde R.: On understanding of land-ocean CO2 contrast over Bay of Bengal: A case study during 2009 summer monsoon, Environmental Science and Pollution Research, 21-7, 5066-5075, doi: 10.1007/s11356-013-2386-2, 2014.

Reddy, B. S. K., Reddy, L.S.S., Cao J., Kumar, K. R., Balakrishnaiah, G., Gopal, K. R, Reddy, R. R., Narasimhulu K., Lal, S., Ahammed Y. N.: Simultaneous Measurements of Surface Ozone at Two Sites over the Southern Asia: A Comparative Study, Aerosol and Air Quality Research, 11: 895–902, doi: 10.4209/aaqr.2011.05.0061, 2011.

Rolph, G.D.: Real-time Environmental Applications and Display sYstem (READY) Website (http://www.arl.noaa.gov/ready.php), NOAA Air Resources Laboratory, Silver Spring, MD., 2003.

Sahu, L.K., Lal, S., and Venkataramani, S.: Distributions of O_3, CO and hydrocarbons over the Bay of Bengal: a study to assess the role of transport from southern India and marine regions during Septembere October 2002, Atmos. Environ., 40, 4633-4645, 2006.

Sawa, Y., et al.: Widespread pollution events of carbon monoxide observed over the western North Pacific during the East Asian Regional Experiment (EAREX) 2005 campaign, J. Geophys. Res., 112, D22S26, doi:10.1029/2006JD008055, 2007.

Scheeren, H. A., Lelieveld, J., Roelofs, G. J., Williams, J., Fischer, H., de Reus, M., de Gouw, J. A., Warneke, C., Holzinger, R., Schlager, H., Klüpfel, T., Bolder, M., van der Veen, C., and Lawrence, M.: The impact of monsoon outflow from India and Southeast Asia in the upper troposphere over the eastern Mediterranean, Atmos. Chem. Phys., 3, 1589-1608, doi:10.5194/acp-3-1589-2003, 2003.

Schell, B., Ackermann, I. J., Hass, H., Binkowski, F. S., and Ebel, A.: Modeling the formation of secondary organic aerosol within a comprehensive air quality model system, J. Geophys. Res., 106, 28275–28293, 2001.

Seinfeld, J.H., and Pandis, S.N.: Atmospheric Chemistry and Physics: from air pollution to climate change, 2nd ed., Wiley-Interscience publication, USA, 2006.

Smit, H.G.J., Straeter, W., Johnson, B.J., Oltmans, S., Davies, J., Tarasick, D.W., Hoegger, B., Stubi, R., Schmidlin, F., Northam, T., Thompson, A.M., Witte, J.C., Boyd, I., Posny, F.: Assessment of the performance of ECC-ozonesondes under quasi-flight conditions in the environmental simulation chamber: insights from the Juelich Ozone SondeIntercomparison Experiment (JOSIE), J. Geophys. Res. 112, D19306. http://dx.doi.org/10.1029/2006JD007308, 2007.

Sprenger, M., Wernli, H., Bourqui, M.: Stratosphere-Troposphere exchange and its relation to potential vorticity streamers and cutoffs near the extratropical tropopause, Journal of Atmospheric Science 64, 1587-1604, 2007.

Srivastava S., S. Lal, S. Venkataramani, S. Gupta, and Acharya Y. B., Vertical distribution of ozone in the lower troposphere over the Bay of Bengal and the Arabian Sea during ICARB-2006: Effects of continental outflow, J. Geophys. Res., 116, D13301, doi:10.1029/2010JD015298, 2011.

Srivastava, S., S. Lal, S.Venkataramani, S. Gupta, andSheelV.: Surface distributions of O_3, CO and hydrocarbons over the Bay of Bengal and the Arabian Sea during pre-monsoon season, Atmos. Environ., 47, 459–467, doi:10.1016/j.atmosenv.2011.10.023, 2012.

Stockwell, W. R., P. Middleton, J. S. Chang, and Tang X.: The second generation regional acid deposition model chemical mechanism for regional air quality modeling, J. Geophys. Res., 95(D10), 16343–16367, doi:10.1029/JD095iD10p16343, 1990.

Subrahamanyam D. B., T. J. Anurose, N. V. P. Kiran Kumar, M. Mohan, P. K. Kunhikrishnan, S. R. John, S. S. Prijith, and Dutt C.B.S.: Spatial and temporal variabilities in vertical structure of the Marine Atmospheric Boundary Layer over Bay of Bengal during Winter Phase of Integrated Campaign for Aerosols, gases and

Radiation Budget, Atmospheric Research, Volume 107, 178-185, doi: 10.1016/j.atmosres.2011.12.014, 2012.

Tanimoto, H., et al.: Direct assessment of international consistency of standards for ground-level ozone: Strategy and implementation toward metrological traceability network in Asia, J. Environ. Monit., 9, 1183– 1193, doi:10.1039/b701230f, 2007.

Tiwari Y. K. and RaviKumar K.: Glass flask air sample analysis through gas chromatography in India: implications for constraining CO2 surface fluxes, WMO/GAW Report No. 194, WMO/TD-No.1553, April 2011, 2011.

World Health Organization, Environmental Health Criteria 213, Carbon monoxide, 1999.

Wiedinmyer, C., S. K. Akagi, R. J. Yokelson, L. K. Emmons, J. A. Al-Saadi, J. J. Orlando, and Soja, A.J.: The Fire Inventory from NCAR (FINN): a high resolution global model to estimate the emissions from open burning, Geosci. Model Dev., 4, 625–641, doi:10.5194/gmd-4-625-2011, 2011.

Zhang, Q., D. G. Streets, G. R. Carmichael, K. B. He, H. Huo, A. Kannari, Z. Klimont, I. S. Park, S. Reddy, J. S. Fu, D. Chen, L. Duan, Y. Lei, L. T. Wang, and Yao Z. L.: Asian emissions in 2006 for the NASA INTEX-B mission, Atmos. Chem. Phys., 9, 5131-5153, doi:10.5194/acp-9-5131-2009, 2009.

Tables

Table 1. The WRF-Chem options used for parameterization of atmospheric processes.

Atmospheric Process	**Scheme used**	**Features of the scheme**
Cloud microphysics	Lin et al. scheme (Lin et al., 1983)	Sophisticated parameterization including ice, snow and graupel processes, suitable for high-resolution simulations.
Longwave radiation	Rapid Radiative Transfer Model (RRTM; Mlawer et al., 1997)	Accurate scheme utilizes look-up tables for efficiency, accounts for multiple bands and microphysical properties.
Shortwave radiation	Goddard shortwave scheme (Chou and Suarez, 1994)	Two-stream multi-band scheme using O_3 from climatology and includes cloud effects
Surface Layer	Monin–Obukhov scheme (Janjic, 1996)	Based on Monin-Obukhov with Zilitinkevich thermal roughness length and standard similarity functions from look-up tables
Land surface option	Noah Land Surface Model (Chen and Dudhia, 2001)	Unified NCEP/NCAR/AFWA scheme with soil temperature and moisture in four layers, fractional snow cover and frozen soil physics. This includes the modifications for better representation of processes over ice sheets and snow covered areas.
Urban surface physics	Urban Canopy Model	3-category urban canopy model with surface effects for roofs, walls and streets.
Planetary boundary layer	Mellor–Yamada–Janjic scheme (Janjic, 2002)	One-dimensional prognostic turbulent kinetic energy scheme, local vertical mixing is included.
Cumulus parameterization	Grell 3D Ensemble scheme (Grell, 1993; Grell and Devenyi, 2002)	Improved version of the GD scheme suitable for coarse as well as high resolution simulations

745

Table 2. A comparison of averaged surface O_3 mixing ratios measured at various sites during summer monsoon period. *boundary layer O_3 over the Arabian Sea.

Observation site	**Longitude (° E)**	**Latitude (° N)**	**Observation period**	**Surface Daytime O_3 (Mean ± Standard Deviation)**	**Reference**
Arabian Sea					
Arabian Sea	69 –76	9 –19	July–August 2002	9	Ali et al., 2009
Western coast of India					
Thiruvananthapuram	76.9	8.5	August 2009	23±7	Present Study
Thiruvananthapuram	76.9	8.5	June–August 2008	19±6	David and Nair, 2011
Kannur	75.4	11.9	July 2010–2011	11±4	Nishanth et al., 2014
MtAbu (1.6km amsl)	72.7	24.6	August 1993–2000	25±9	Naja et al., 2003
Ahmedabad	72.6	23	July 1991–1995, August 1991–1995, July–August 2003–2007	22±8, 17±4, 25*	Lal et al., 2000; Srivastava et al., 2012
Central India					
Anantpur	77.65	14.62	July 2009	30±2	Reddy et al., 2011
Eastern coast of India					
Bhubaneswar	86.4	20.5	June–August 2011–2012	29±6	Mahapatra et al., 2014
Bay of Bengal					

Bay of Bengal	80.3–90.1	11–21.1	July–August 2009	30±7	Present Study

Table 3. A comparison of mean values from observations with model-simulated parameters along with the mean bias. The squared correlation coefficients correspond to the linear regression analysis between daily averaged in situ and simulated parameters.

Parameter	**Observation**	**Model (WRF-Chem)**	**Mean bias**	**R^2**
Pressure (hPa)	1001.3±2.1	999.4±2.2	-1.9	0.93
Temperature (°C)	29.3±0.9	28.7±0.6	-0.6	0.13
Relative Humidity (%)	87.9±4.2	86.8±2.8	-1.1	0.36
O_3 (nmol mol^{-1})	29.7±6.8	31.6±6.6	1.9	0.58
CO (nmol mol^{-1})	96±25	114±30	18	0.19

Table 4. A comparison of average mixing ratios of surface trace gases measured over northern BoB (81-91° E, 16-21.5° N) and central BoB (80-91° E, 11-16° N) in different seasons as measured during different experiments. The range of mixing ratios (i.e. minima–maxima) is given in the brackets. *CO mixing ratios below the detection limit (i.e. 50 nmol mol^{-1}) are not considered in the analysis.

Study period	**Name of Experiment**	**Reference**	**O_3 (nmol mol^{-1}) over northern BoB**	**O_3 (nmol mol^{-1}) over central BoB**	**CO (nmol mol^{-1}) over northern BoB**	**CO (nmol mol^{-1}) over central BoB**	**CH_4 (µmol mol^{-1}) over northern BoB**	**CH_4 (µmol mol^{-1}) over central BoB**
December 2008–January 2009	W_ICARB	David et al., 2011	63.0±4.7 (50.8–73.8)	40.9±6.7 (27.7–63.5)	302±68 (140–450)	188±53 (50–320)	No data	No data
February 2003	BOBEX-II	Lal et al., 2007	~34.1 (15.8–50.4)	~26.8 (13.9–35.0)	~238 (187–292)	~192 (159–224)	~1.77 (1.70–1.85)	~1.73 (1.68–1.77)
February–March 2001	BOBEX-I	Lal et al., 2006	~23.8 (16.1–38.3)	~38.0 (19.4–62.9)	~194 (165–235)	~227 (97–339)	~1.94 (1.89–2.02)	~1.91 (1.74–2.06)
March–April 2006	ICARB	Nair et al., 2011; Srivastava et al., 2012	27.4±2.9 (21.4–32.6)	13.4±4.2 (3.1–24.6)	~189 (157–235)	~132 (96–167)	~1.84 (1.80–1.88)	~1.80 (1.75–1.84)
July–August 2009	CTCZ	Present Study	30.0±6.9 (8.50–54.1)	27.5±5.0 (8.8–40.5)	95±25 * (50-198) *	101±27 * (50-157) *	1.86 ±0.12 (1.62–2.15)	1.72±0.14 (1.57–1.96)
September–October 2002	BOBPS	Sahu et al., 2006	~27.3 (17.8–33.8)	~30.6 (22.5–35.2)	~152 (109–179)	~141 (108–211)	~1.79 (1.72–1.86)	~1.73 (1.68–1.80)
November 2010	-	Mallik et al., 2013	~46.0 (26.7–59.6)	~38.7 (17.8–60.8)	~223 (131–280)	~188 (42–266)	~1.95 (1.85–2.06)	~1.79 (1.67–1.93)

Figures

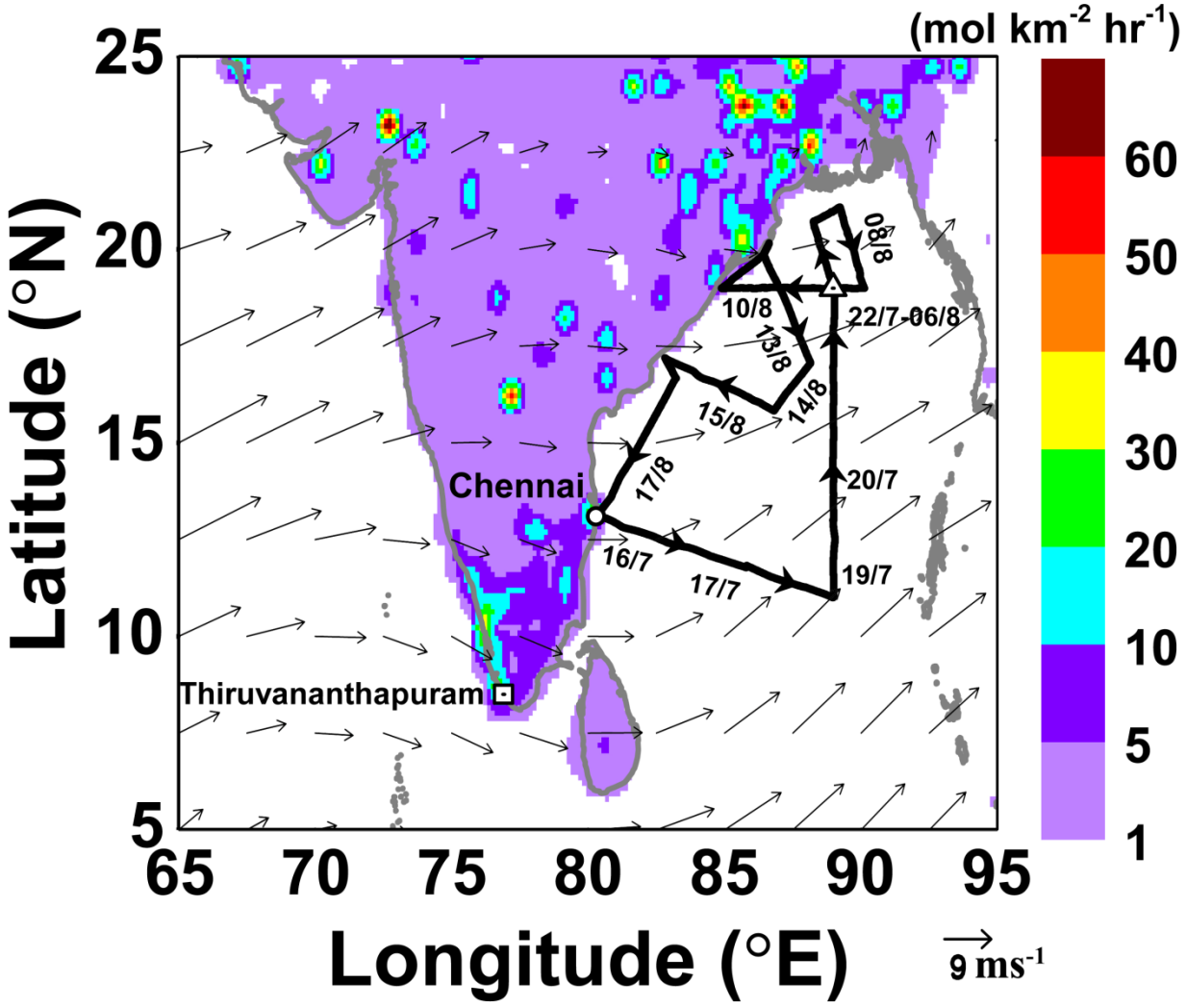

Figure 1. Cruise track (continuous black line) of the Research Vessel *Sagar Kanya* along with synoptic winds at 925 hPa (black thin arrows) and NO_x emissions in background colour map. The dates corresponding to approximate ship positions are marked along the track. The start and end position of the cruise, stationary position of the ship, and Thiruvananthapuram are shown by the circle, triangle and square respectively.

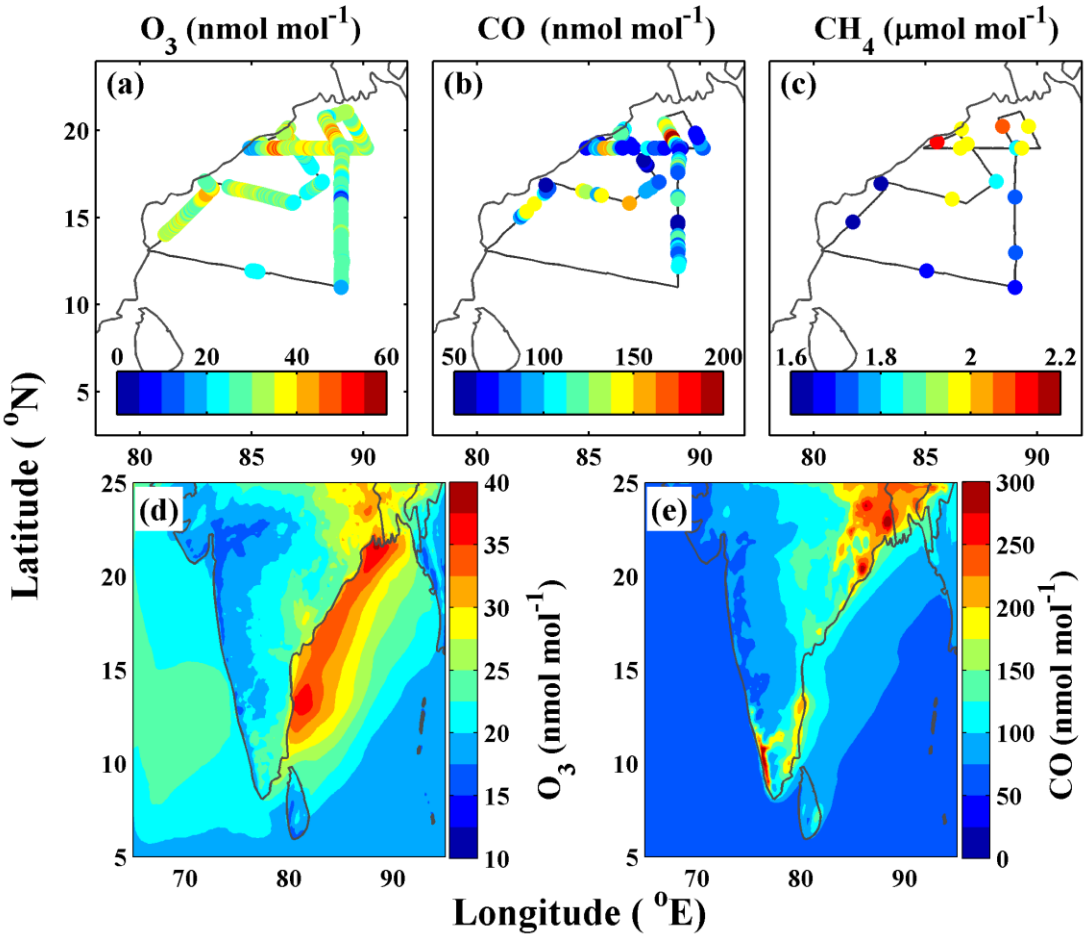

Figure 2. Spatial variation of surface O_3 (a), CO (b), and CH_4 (c) mixing ratios along the cruise track during the CTCZ campaign. WRF-Chem-simulated spatial distribution of surface O_3 (d) and CO (e) averaged during the July 16–August 17, 2009 period.

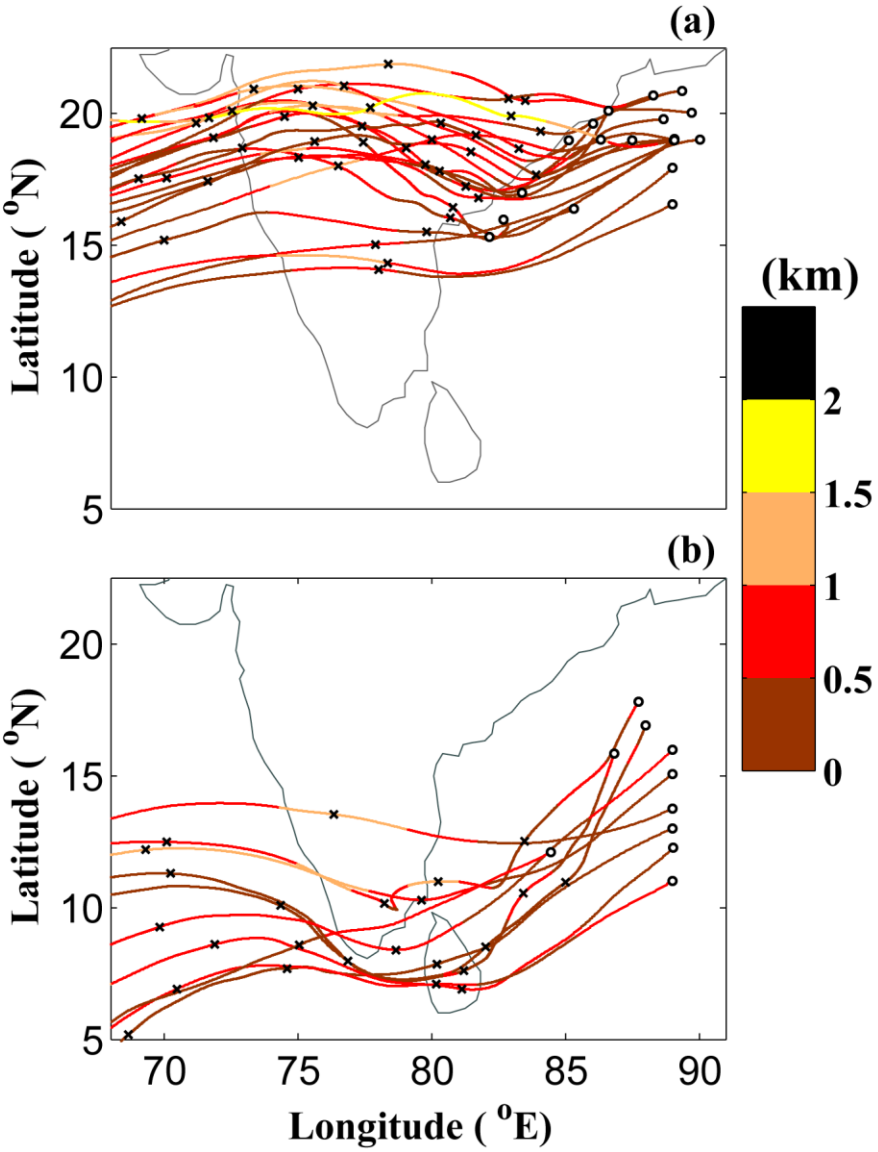

Figure 3. Five-day airmass back-trajectories during the study period ending at the measurement locations (small black circles) grouped for corresponding airmasses from (a) central/northern India and (b) southern India. The cross symbols along the trajectories represent each back-day. The colour scale shows the height (in km) of the trajectories.

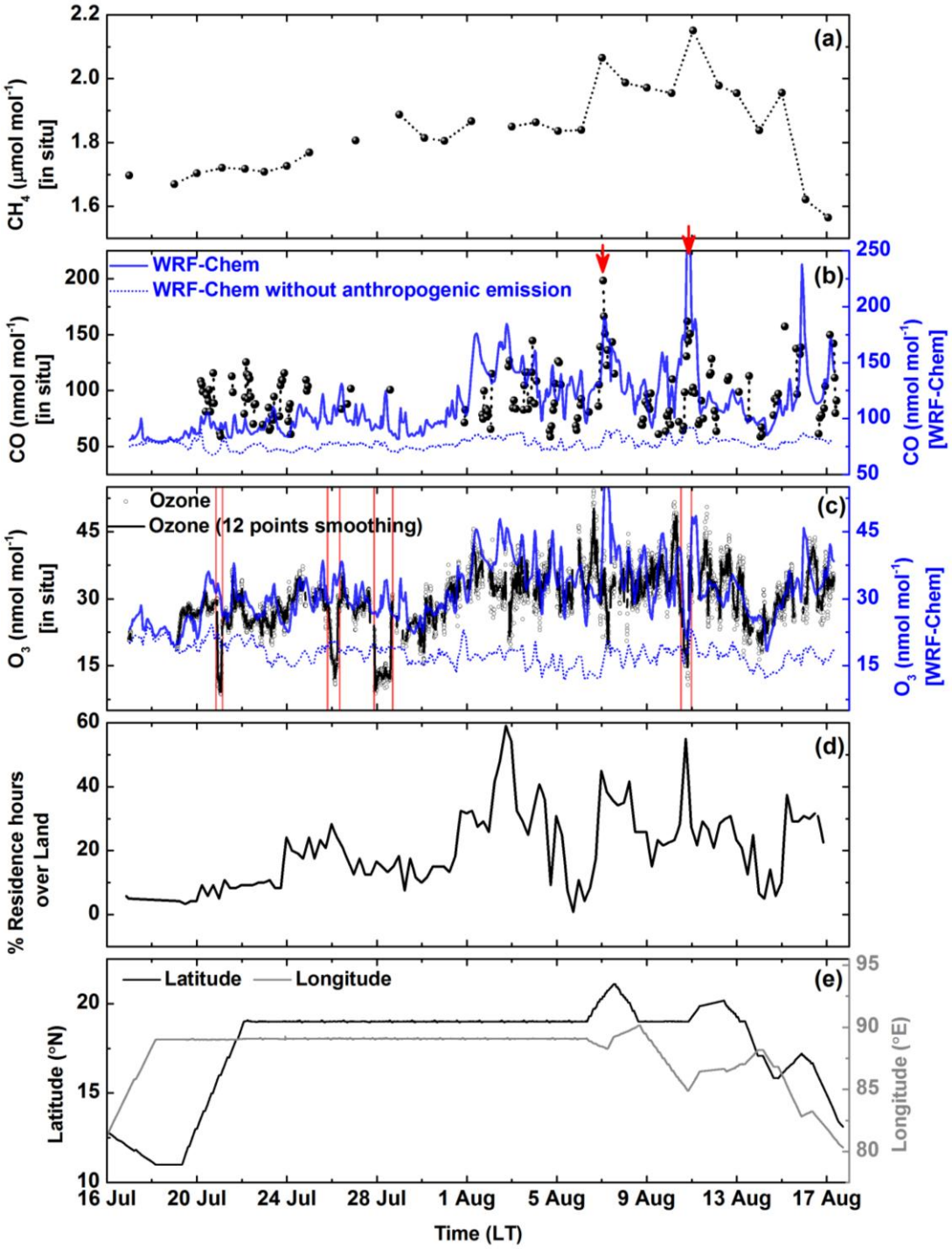

785 **Figure 4**. Variations in observed CH_4 (a), CO (b), O_3 (c), and percentage residence time over land (d) along with WRF-chem simulated O_3 and CO (blue line) during the campaign. Events of sharp decrease in O_3 during rainfall are marked by vertical red lines (Fig. 8). (e) Variations in measurement locations.

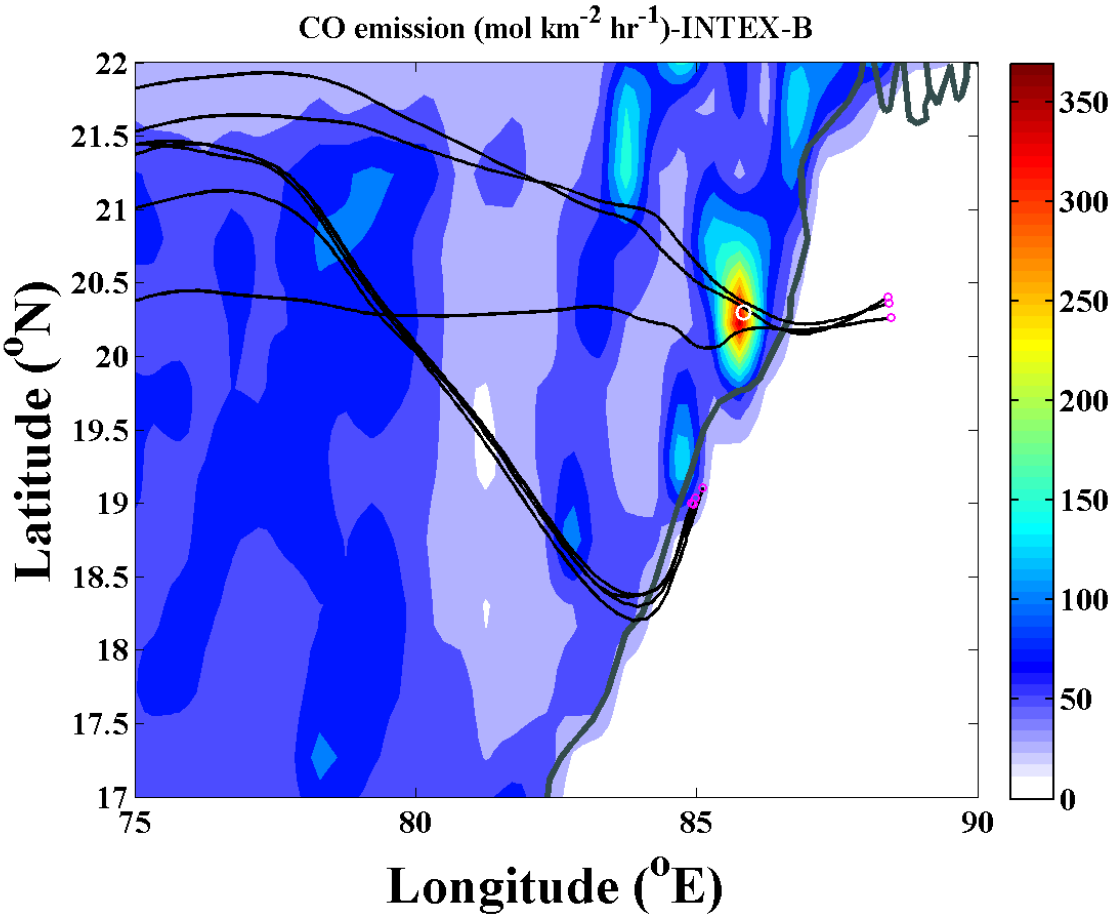

790 **Figure 5.** Backward airmass trajectories (black curves) 500 m above the location of higher CO observations as marked by red arrows in Fig. 4b during August 7 and 11, 2009. The background colour map shows the spatial distribution of anthropogenic CO emissions over the Indian region for the year 2006 from INTEX-B inventory. The small circles in magenta represent the points where observations were made, as well as the end-point of trajectories. The white circle over the hot-spot region denotes an observational site, Bhubaneswar.

795

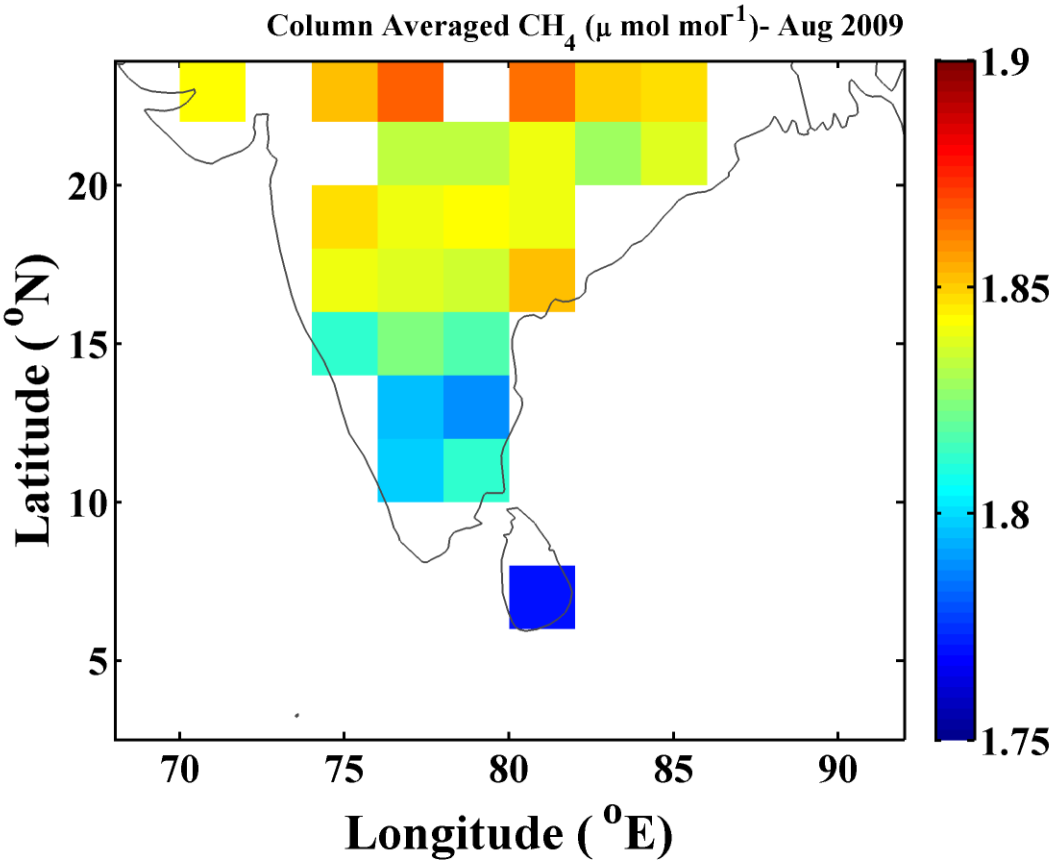

Figure 6. Spatial distribution of column averaged CH_4 for the month of August 2009 as obtained from SCIAMACHY.

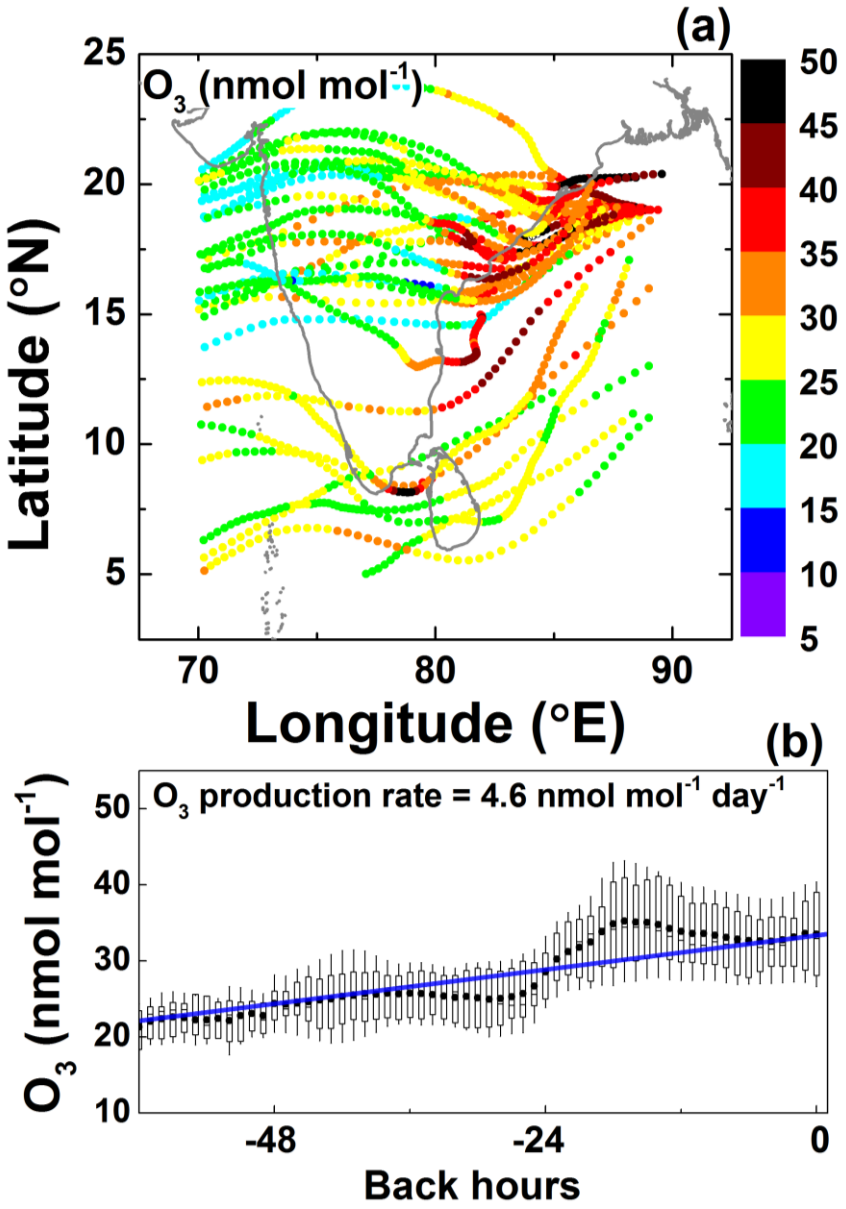

Figure 7. (a) WRF-Chem simulated O_3 along the airmass trajectories ending over a few representative locations over the BoB. (b) Variation of O_3 mixing ratios with time along the trajectories as shown in 7a. In box plot, the black dots and lines inside the box represent the mean and median of the data respectively. While the lower and upper edges of boxes represent the 25th and 75th percentiles respectively, the whiskers represent standard deviations.

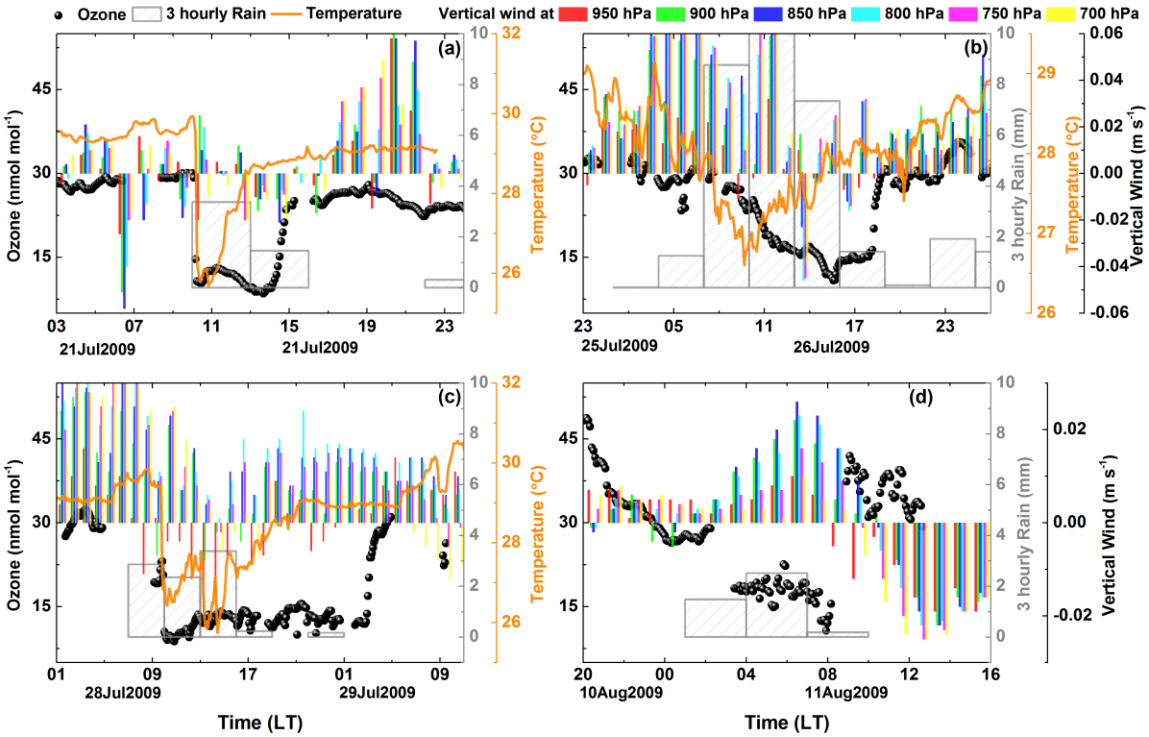

Figure 8. Surface O_3 (black dots) along with temperature (orange curve) and 3-hourly rainfall (grey vertical bar) during the four events of sharp decline in O_3 (a–d) as marked in Fig. 4c. Colours indicate the vertical wind as simulated by WRF-Chem.

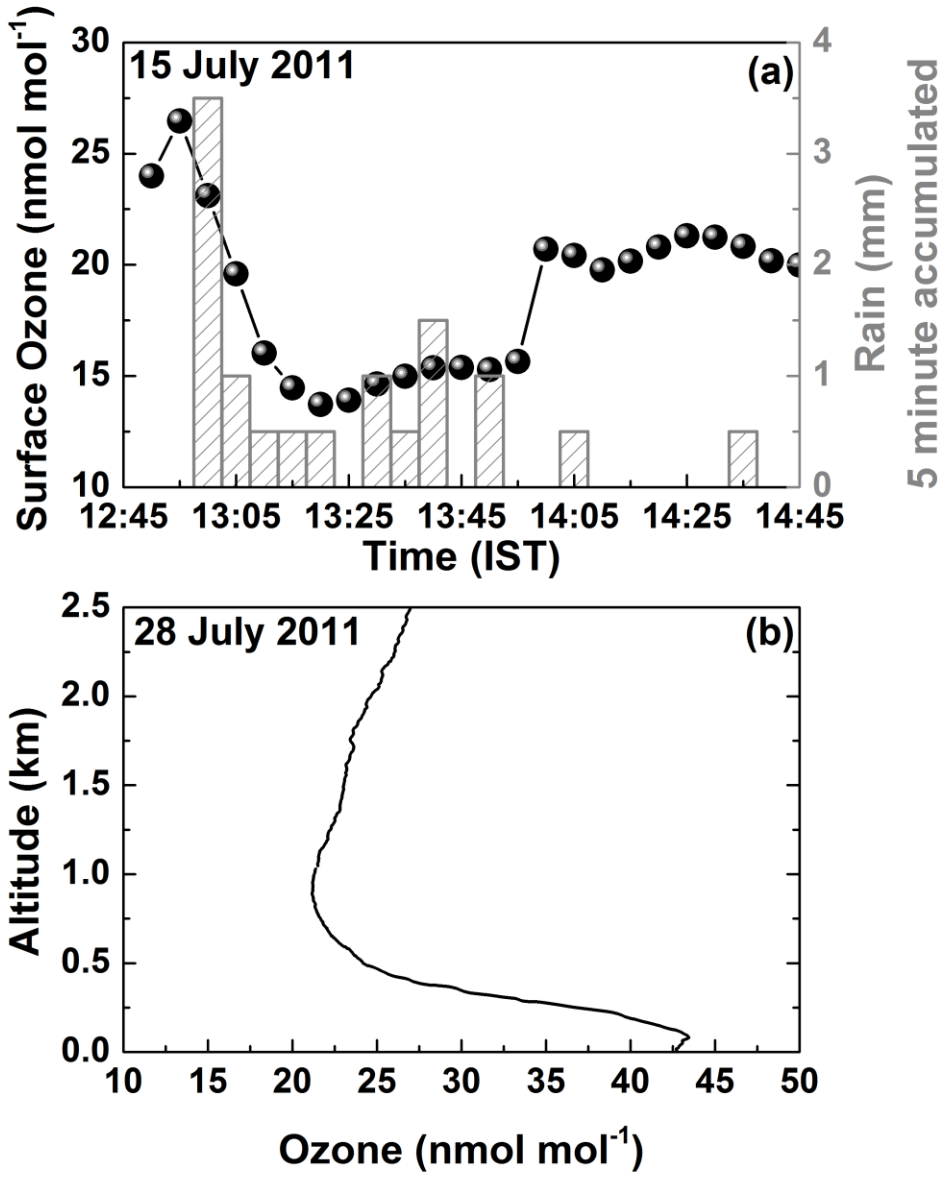

815

Figure 9. (a) Temporal variation in surface O_3 mixing ratio (black dots) along with 5-minute accumulated rainfall (grey vertical bars) over Thumba, Thiruvananthapuram (location of the site shown in Fig. 1) on 15 July 2011. (b) Vertical profile of O_3 mixing ratio over Thumba, Thiruvananthapuram as measured on 28 July 2011.

820

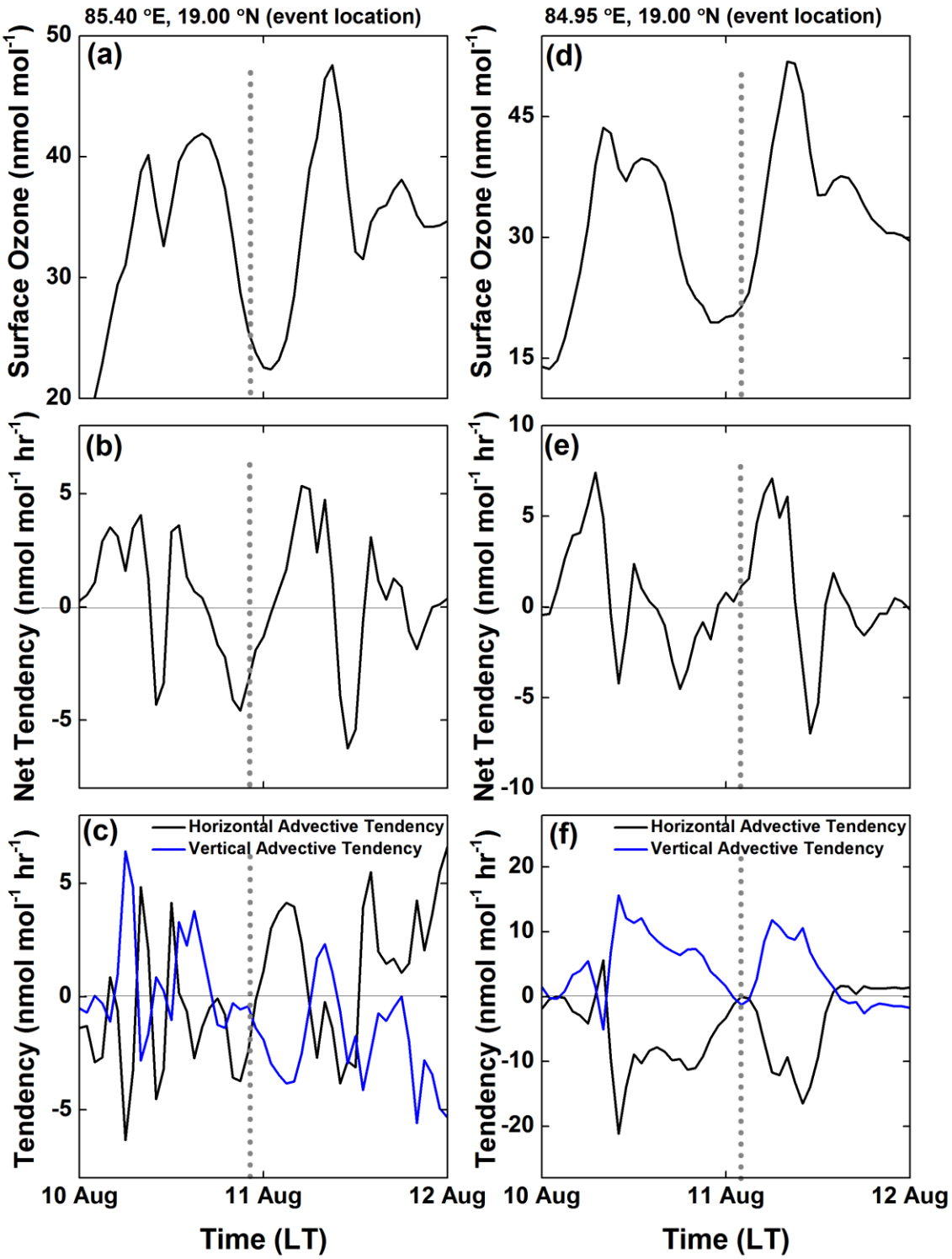
85.40 °E, 19.00 °N (event location)
84.95 °E, 19.00 °N (event location)
(a)
(b)
(c)
(d)
(e)
(f)
Surface Ozone (nmol mol-1)
Net Tendency (nmol mol-1 hr-1)
Tendency (nmol mol-1 hr-1)
Horizontal Advective Tendency
Vertical Advective Tendency
10 Aug
11 Aug
12 Aug
Time (LT)

Figure 10. Time series of surface O_3 (a) and various tendency terms (b and c) over the event location during the fourth low-O_3 event, as obtained from WRF-Chem simulations. 10d–f are the same as 10a–c, but for another location during the same event. These two event locations are also marked by triangles in Figure 11. Vertical dotted line shows the time of the event in the in situ observations of surface O_3 over the indicated locations.

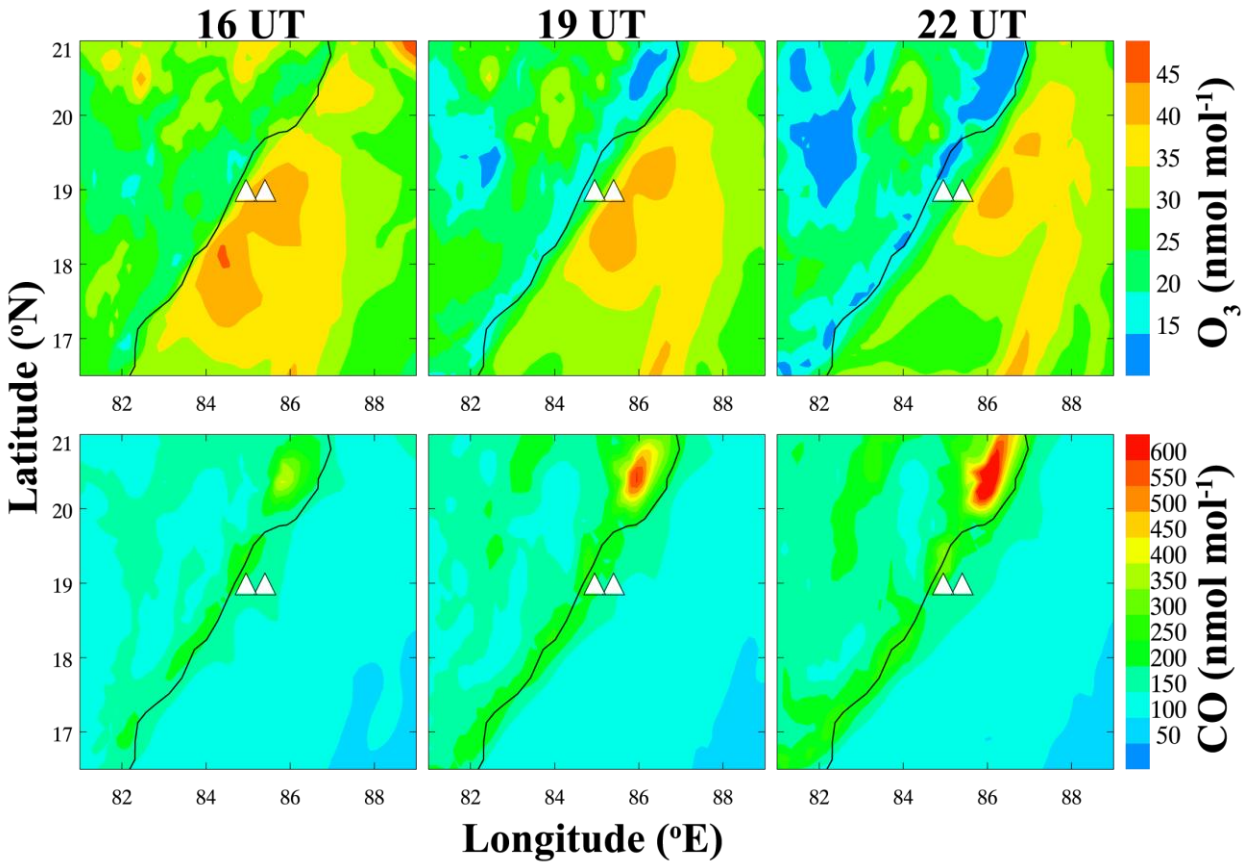

Figure 11. Spatial distribution of surface O_3 (top panel) and CO (bottom panel) at 16:00 UT and 19:00 UT on August 10, 2009, both prior to and during the fourth event, which took place 22:00 UT on August 10, 2009. White triangles show two locations (85.40° E, 19.00° N; 84.95° E, 19.00° N) corresponding to the event.

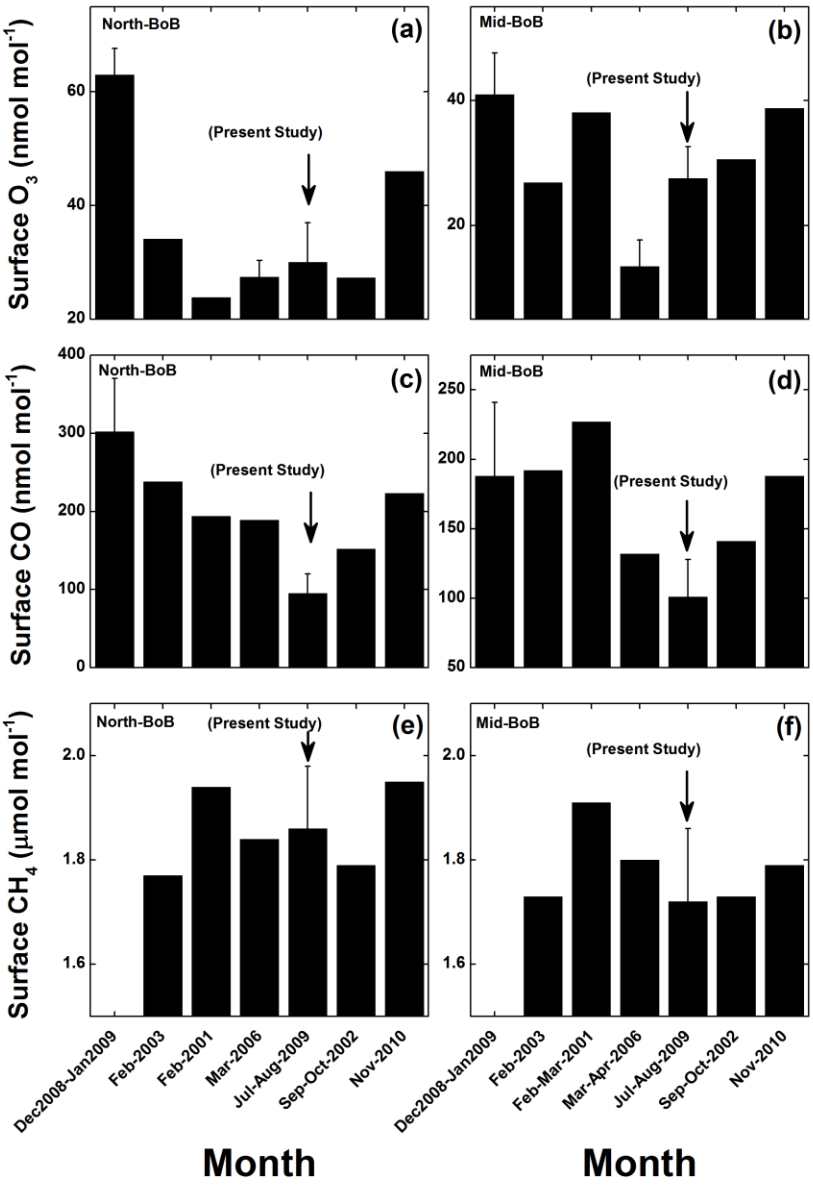

Figure 12. Seasonal variation in average O_3, CO, and CH_4 mixing ratios over (a, c, e) northern BoB and (b, d, f) central BoB. Except for July–August 2009 (present study period), all average values are obtained from the literature (David et al., 2011; Lal et al., 2007; Lal et al., 2006; Nair et al., 2011; Srivastava et al., 2012; Sahu et al., 2006; and Mallik et al., 2013). Error bars show standard deviations for respective study periods. For any points for which high resolution measurements are not available, standard deviations are not shown.